

University of California

Los Angeles

**Finite-Element Elasto-Plastic Stress Analysis of the  
Helium-cooled Pebble Bed Blanket Concept**

A project submitted in partial satisfaction  
of the requirements for the degree Master of Science  
in Mechanical Engineering

by

Patrick Chalit Pattamanuch

**2004**

The project of Patrick Chalit Pattamanuch is approved.

---

Gregory P. Carman

---

Daniel Yang

---

Nasr M. Ghoniem, Committee Chair

University of California, Los Angeles

2004

For my parents.

# TABLE OF CONTENTS

LIST OF FIGURES & TABLES .....	iv
ACKNOWLEDGEMENTS .....	vi
ABSTRACT OF THE PROJECT.....	vii
1. INTRODUCTION .....	1
1.1. A Brief Introduction to Fusion Reactor Research and Design .....	1
1.2. A Brief Overview of Fusion Reactor Principles and Components .....	2
1.3. Project Objectives .....	5
2. BLANKET BREEDER REQUIREMENTS .....	7
3. HELIUM-COOLED PEBBLE BED (HCPB) CONCEPT .....	8
3.1. Box Design.....	8
3.2. Coolant Flow.....	11
4. ANALYSES SET UP .....	12
4.1. Objectives.....	12
4.2. Model Setup .....	12
4.2.1. Solid Modeling.....	12
4.2.2. ANSYS Implementation, Element Type, and Model Meshing .....	13
4.2.3. Material Models .....	16
4.2.3.1. Elastic Material Model.....	16
4.2.3.2. Elasto-plastic Material Model.....	17
4.2.4. Boundary Conditions .....	18
4.2.5. Pressure Load Application.....	20
5. RESULTS & DISCUSSION.....	23
5.1. Elastic Analysis.....	23
5.1.1. Deformation Results .....	23
5.1.2. Von Mises Stress Results .....	24
5.2. Elasto-plastic Analysis .....	25
5.2.1. Deformation Results .....	26
5.2.2. Von Mises Stress Results .....	26
5.3. Elastic versus Elasto-plastic Results .....	27
5.4. Step Loading Results .....	38
5.4.1. Displacement and Strain Results .....	45
5.4.2. Stress Results .....	45
6. SUMMARY & CONCLUSIONS.....	47
Appendix 1: engineering drawings of model (in mm).....	52
REFERENCES .....	56

## LIST OF FIGURES & TABLES

	<b>Page</b>
<b>Figure 1.2.1:</b> Cutaway view of magnetic confinement fusion reactor concept.	3
<b>Figure 1.2.2:</b> A simplified vertical cross section of a representative fusion reactor.	4
<b>Figure 3.1.1:</b> Helium-cooled pebble bed concept (exploded view).	9
<b>Figure 3.1.2:</b> View of the plates of the stiffening grid.	10
<b>Figure 3.1.3:</b> Breeder unit concept.	10
<b>Figure 4.2.2.1:</b> SOLID95 geometry and nodal configuration.	14
<b>Figure 4.2.2.2:</b> Completed meshed model, using brick and tetrahedral SOLID95 elements.	15
<b>Table 4.3.2.1:</b> Key maximum temperatures in the blanket.	16
<b>Table 4.3.2.1.1:</b> Elastic material model data.	17
<b>Figure 4.3.2.2.1:</b> 450°C True stress-strain curve for F82H.	19
<b>Figure 4.2.5.1:</b> Pressure loading (top view).	20
<b>Figure 4.2.5.2:</b> Pressure loading (bottom view).	21
<b>Table 4.2.5.1:</b> Load stepping scheme for third analysis.	22
<b>Figure 5.1.1.1:</b> Elastic analysis displacement (top view).	29
<b>Figure 5.1.1.2:</b> Elastic analysis displacement (top view).	29
<b>Figure 5.1.1.3:</b> Elastic analysis displacement (isometric/section view).	30
<b>Figure 5.1.1.4:</b> Elastic analysis displacement (section view).	30
<b>Figure 5.1.2.1:</b> Elastic analysis von Mises stress (top view).	31
<b>Figure 5.1.2.2:</b> Elastic analysis von Mises stress (top view).	31
<b>Figure 5.1.2.3:</b> Elastic analysis von Mises stress (isometric/section view).	32
<b>Figure 5.1.2.4:</b> Elastic analysis von Mises stress (section view).	32
<b>Figure 5.1.2.5:</b> Magnified view of maximum von Mises stress location.	33
<b>Figure 5.2.1.1:</b> Elasto-plastic analysis displacement (top view).	34

<b>Figure 5.2.1.2:</b>	Elasto-plastic analysis displacement (top view).	34
<b>Figure 5.2.1.3:</b>	Elasto-plastic analysis displacement (isometric/section view).	35
<b>Figure 5.2.1.4:</b>	Elasto-plastic analysis displacement (section view)	35
<b>Figure 5.2.2.1:</b>	Elasto-plastic analysis von Mises stress (top view).	36
<b>Figure 5.2.2.2:</b>	Elasto-plastic analysis von Mises stress (top view).	36
<b>Figure 5.2.2.3:</b>	Elasto-plastic analysis von Mises stress (isometric/section view).	37
<b>Figure 5.2.2.4:</b>	Elasto-plastic analysis von Mises stress (section view).	37
<b>Figure 5.4.1:</b>	Evolution of maximum nodal displacement as a function of helium coolant pressure.	39
<b>Figure 5.4.2:</b>	Evolution of maximum nodal strain as a function of helium coolant pressure.	40
<b>Figure 5.4.3:</b>	Evolution of maximum nodal von Mises stress as a function of helium coolant pressure.	41
<b>Figure 5.4.4:</b>	Evolution of HCPB box displacement (m) with increasing pressure.	42
<b>Figure 5.4.5:</b>	Evolution of HCPB box strain with increasing pressure.	43
<b>Figure 5.4.6:</b>	Evolution of HCPB box von Mises stress (MPa) with increasing pressure.	44

## ACKNOWLEDGEMENTS

First, I would like to thank Professor Ghoniem for his guidance, patience, and vision in helping me with this project. His vast experience and knowledge have been invaluable to me in my work, both in the classroom and with regard to my project. Additionally, I would like to thank Dr. Shahram Sharafat for meeting with me whenever I needed help with ANSYS, Solidworks, and the numerous problems I had during the course of this project. The effort and hours he has generously provided will be appreciated for a very long time to come. Finally, I would like to extend a great deal of gratitude to the other members of the Computational Nano- and Micromechanics Lab who have helped me with my work—without them this project would not have been possible.

Additionally, I would like to thank Professor Carman and Professor Yang for their efforts as my nominating committee.

# **ABSTRACT OF THE PROJECT**

## **Finite-Element Elasto-Plastic Stress Analysis of the Helium-cooled Pebble Bed Blanket Concept**

**By**

**Patrick Chalit Pattamanuch**

**Master of Science in Mechanical Engineering**

**University of California, Los Angeles**

**2004**

**Professor Nasr M. Ghoniem, Chair**

This project consists of finite-element analyses of the structural-mechanical behavior of the helium-cooled pebble bed (HCPB) blanket concept. The HCPB blanket is an integral component of future fusion reactor designs, and these analyses were completed as part of a verification of the HCPB concept function and performance under faulted conditions. Specifically, the finite-element analyses will show whether or not the HCPB concept will be able to withstand a box pressurization to the level of the helium coolant pressure of 8 MPa in the case of an internal leak.

The analyses were completed using two different material properties assumptions, whose distinctions are important to the project. The first is elastic, where the material is assumed to be purely elastic, without consideration of plasticity effects. The second is elasto-plastic, which assumes a material that behaves according to a true stress-strain curve; that is, plasticity effects are considered. A comparison of the results of these two different analyses will provide an insight into the importance of using the more realistic material model of elasto-plasticity over the simpler elastic case. Both cases were computed under a constant pressure load of 8 MPa.

Another analysis, which uses elasto-plastic material properties, was completed using stepped, constant loading past 8 MPa. The purpose here was to ascertain the limit of elastic behavior in the HCPB concept, if any.

All analyses were performed using a commercial finite-element computing package known as ANSYS. Finite-element modeling setup is discussed, and the necessary assumptions and implemented data are presented and tabulated. The three analyses were solved in ANSYS and the resulting data is presented.

The results of these finite-element analyses indicate that the HCPB concept will be able to withstand a box pressurization of 8 MPa in the case of an internal leak, and that the structural-mechanical behavior of the HCPB concept will remain elastic up to a box pressure of roughly 10 MPa before nonlinear stress behavior occurs. Contour plot data

show that the most significant deformation occurs in the sidewall of the HCPB design, though the magnitude of this deformation is not significant. Areas of plasticity appear in the results, but these have been disregarded as exaggerated due to the nature in which ANSYS treats stress concentrations at sharp edges and corners.

# 1. INTRODUCTION

## 1.1. A Brief Introduction to Fusion Reactor Research and Design

Our survival on earth is due mostly to the energy and warmth given to us by the sun. As in all other stars in our universe, ours is powered by fusion, a process where hydrogen atoms combine to form helium and an enormous amount of energy, and it has long been a dream of engineers, physicists, and other researchers to harness the near-infinite well of energy that fusion may provide for mankind's growing energy consumption needs. Though the physical nature of fusion has been known for decades, the technology that is needed for its feasibility has not yet come to fruition, as may be seen in the decades of iterative reactor designs and subsequent revisions. In short, the amount of work that has been completed—as well as the research and development that is needed—is enormous. So why, then, is fusion such a daunting task? The short answer is that fusion reactor technology is enormously complex, such that it requires expertise in all fields of engineering for successful implementation, and a wide variety of challenges must then be overcome: new materials development, structural and thermal stresses, heat transfer, manufacturing, maintenance, magnetohydrodynamic (MHD) effects, electromagnetics, economic feasibility, power conversion systems, plasma and nuclear physics—the list goes on. And thus, because the challenges are so numerous and so novel, a vast community of researchers exists today working toward developing fusion technology

together, where experts from all fields contribute to the eventual reality of fusion as an alternate solution to earth's demand for power, through their ingenuity and hard work.

## **1.2. A Brief Overview of Fusion Reactor Principles and Components**

Two main concepts for fusion reactor design exist currently: inertial confinement and magnetic confinement. Because this project deals only with fusion research as it pertains to magnetic confinement, inertial confinement will not be discussed here. In the following, the main components and principles of magnetic-confinement fusion will be discussed.

Shown in figure 1.2.1 is a cutaway view of a simplified fusion reactor. In figure 1.2.2, a vertical cross section of a similar fusion reactor is shown. In the magnetic confinement design, the reactor takes the general shape of a hollow torus, where a plasma occupies the hollow space as indicated in both figures 1.2.1 and 1.2.2. The plasma is a super-hot (>15000K) cloud of ionized gas, where isotopes of hydrogen—namely deuterium ( $^2\text{H}$ ) and tritium ( $^3\text{H}$ )—are fused together, releasing energized alpha particles, neutrons, and heat.

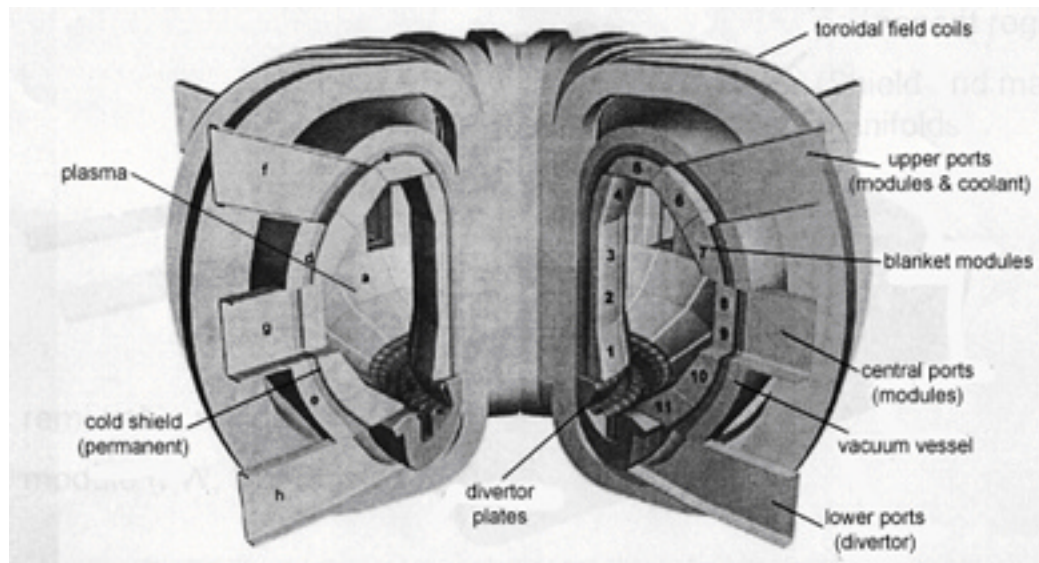


**Figure 1.2.1.** Cutaway view of magnetic confinement fusion reactor concept.  
Taken from [4].

Because of its ionized state, the plasma's shape and size can be controlled using a complex system of powerful electromagnetic coils that produce fields in both the toroidal and poloidal magnetic field directions. These magnets control and confine the plasma shape inside the fusion reactor such that the plasma does not touch any of the reactor's surfaces, since a plasma at temperatures in excess of 15000K would vaporize virtually all materials. The first wall of the reactor is the surface that is in closest proximity to the plasma, and as such it receives the highest heat flux, as well as the highest amount of radiation damage from neutrons, with energies of up to 14 MeV. In many designs, the first wall and other hot components are cooled by high-pressure, high-flow-rate helium gas, which is subsequently taken to a heat exchanger to create steam for power conversion.

Behind the first wall is the first wall blanket breeder, where tritium fuel is produced. The blanket breeder is necessary because of the extreme scarcity of natural tritium on earth,

such that fusion technology would not be feasible without its own tritium-producing capability. Contained within the breeder is a lithium-containing compound that breaks down into tritium when reacted with the energetic neutrons that come out of the plasma as a reaction byproduct. The tritium is then extracted out of the blanket and collected, with a purge gas, such as helium in many designs, but it must be stored carefully because it is radioactive and has a half-life of about 12.3 years. This project deals with a very specific blanket breeder design, where the blanket modules contain small lithium-ceramic pebbles, as well as beryllium pebbles, the latter of which act as neutron multipliers, further increasing the rate of tritium production. This is the basis of the helium-cooled pebble bed blanket (HCPB) concept.

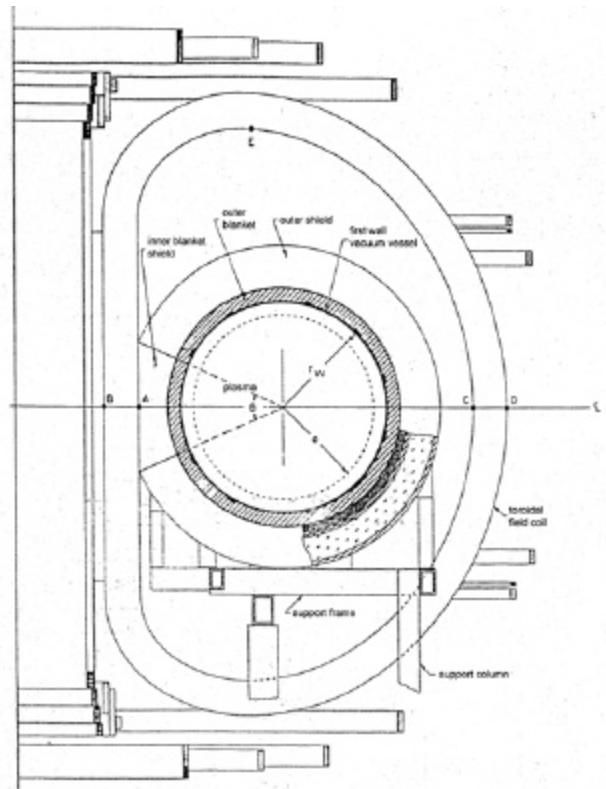


**Figure 1.2.2.** A simplified vertical cross section of a representative fusion reactor. Taken from [5].

In many designs, there lies a vacuum vessel outside of the breeder blanket and first wall. This is critical because the plasma requires a vacuum for a good fuel burn reaction environment. Outside of the vacuum vessel lies a protective outer shield that is meant to protect the magnetic field coils from energetic neutron radiation damage, as well as from radiation heating. Because the field coils will be superconducting—and thus must be refrigerated to only a few degrees Kelvin—heat shielding is very critical in order to prevent huge power losses from cooling the coils. The outer shield also serves the important purpose of shielding personnel and the environment from detrimental neutron radiation.

### **1.3. Project Objectives**

The project consists of analyses of the structural-mechanical behavior of the blanket breeder box—specifically, the helium-cooled pebble bed blanket concept design—under helium coolant pressurization. The analyses will show whether or not the concept design will be able to withstand a box pressurization to the level of the helium coolant pressure of 8 MPa in the case of an internal leak.

The analyses were completed computationally using a commercial finite-element modeling program called ANSYS. In the first analysis, a purely elastic material was assumed, where only a Young's modulus was implemented in the material model, versus the implementation of a true stress-strain curve. In the second analysis, an elasto-plastic—and thus a more realistic—material model was implemented, where a true stress-strain curve was used to describe the material behavior under mechanical loading.

Finally, a third analysis examines the behavior of stress, strain, and displacement as a function of stepped pressure loading of the elasto-plastic case. This last analysis was performed to determine limits of the structure's ability to handle deformation and stress as box pressurization was increased past 8 MPa.

## 2. BLANKET BREEDER REQUIREMENTS

The main requirements observed at the conceptual stage of developing a new design for a blanket breeder should be as follows:

- Meet or exceed the levels of radiation shielding, heat removal, and tritium fuel breeding necessary in a fusion reactor.
- The design must stay below the mechanical and thermal limits of the structural and functional materials.
- Withstand a box pressurization to the coolant pressure level in the case of an internal leak. After such an occurrence, the box can be replaced.
- The design must accommodate an acceptable pressure loss.
- Design to be consistent with existing manufacturing technologies, or describe and define technologies that need to be developed [3].

### **3. HELIUM-COOLED PEBBLE BED (HCPB) CONCEPT**

#### **3.1. Box Design**

The outside shell of the blanket box consists of a steel plate containing internal cooling channels formed into a U-shape, where the two remaining sides are closed by cap plates, which are cooled (see figure 3.1.1). The inlets and outlets for coolant and purge gases are located on the radial portion of the back of the box [3].

A stiffening grid of radial-toroidal and radial-poloidal plates is welded into the box. This grid will be fabricated inside the box by first TIG-welding box-high poloidal plates of the first wall and caps, then welding in the toroidal plates that support the sidewall walls. The joints of each collection of four stiffening plates makes a cross that continues into the radial back; these joints are necessary for a strong connection between the grid and the module back plate. The mechanical strength of the box's walls determined the grid spacing, and thus the optimal spacing was found to be approximately 200mm for HCPB-typical walls. From figure 3.1.2, four circling channels supplied from the radial back pass helium coolant through each stiffening plate [3].

The cellular design of the blanket box offers rectangular space that can contain the functional materials needed for the breeding blanket (i.e. lithium-ceramic and beryllium pebbles). Thus, the breeder units may be thought of as black boxes with piping for helium coolant flow and tritium fuel purging at their radial back. The detailed design of the breeder units—which will contain lithium-ceramic and beryllium pebbles—will not

be discussed here; for now it is assumed that the breeder units will be inserted and fixed into the cells created by the stiffening grid [3]. Figure 3.1.3 shows the breeder unit design in graphic form.

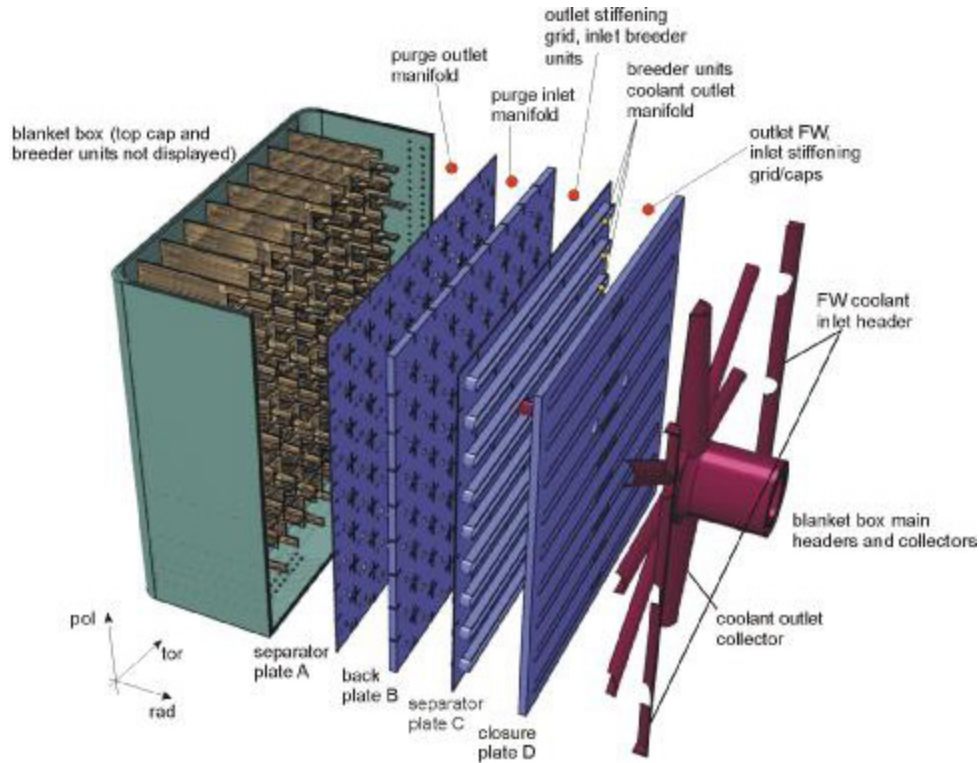


**Figure 3.1.1.** Helium-cooled pebble bed concept (exploded view). Taken from [3].

The back plate portion of the box consists of several large steel plates, creating manifolds that reach all the cells in the box, ensuring their supply of helium coolant and purge gas (see figure 3.1.1). Additionally, two of these plates (C and D in figure 3.1.1) lend the mechanical strength necessary for the mechanical attachment [3].

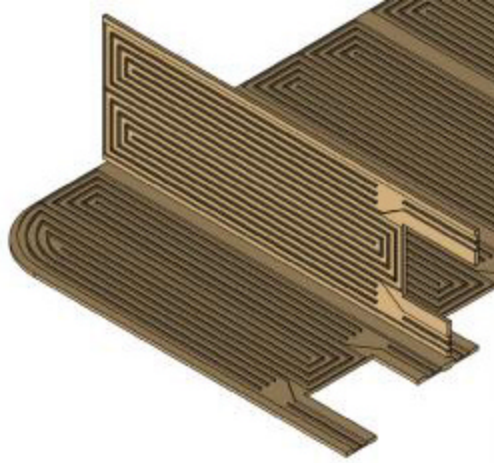


**Figure 3.1.2.** View of the plates of the stiffening grid. Taken from [3].

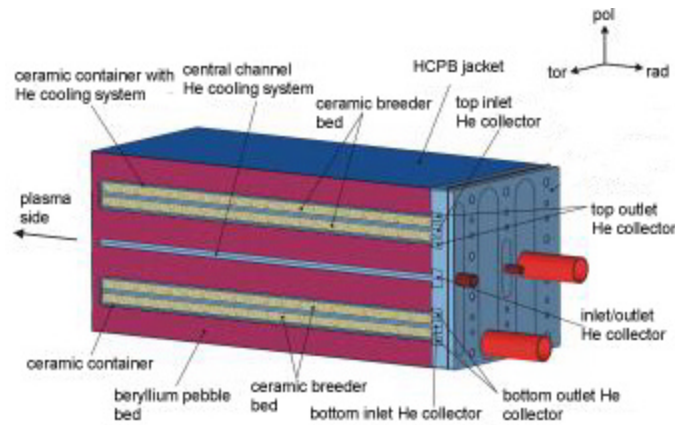


**Figure 3.1.3.** Breeder unit concept. Taken from [3].

The purge system uses the space between the breeder units and the back plate C, with two thin plates that create two distinct headers for the lithium-ceramic breeder and beryllium pebble beds inside the breeder unit, as well as a purge gas collector shared by both. The back plate C and the crosses of the stiffening grid are welded to each other, and this makes up the closing wall of the breeding region. The 8 MPa helium cooling system uses the space between plate C and the closing plate D of the blanket box. Coolant pipes from the stiffening grid and from the inserts penetrate plate C to link up the manifolding.

Toroidal webs connect plates C and D. Besides creating the needed mechanical support, the webs contain a space that is the outlet collector for coolant from the breeder units [3].

### **3.2. Coolant Flow**

One of the challenging tasks in the design of the blanket breeder is ensuring that all structures are supplied with sufficient cooling. In the HCPB design, helium coolant passes the major blanket structures in the following series:

- Through the U-shape first wall/sidewalls
- Through the stiffening grid plates (75%) and the caps (25%) in parallel
- Through the breeder units

As stated before, the helium coolant pressure has been specified at 8 MPa [3]. Note that the coolant does not flow into the box that contains the stiffening grid plates under normal operating conditions. This project deals with the accidental leak of coolant gas into the box area, and seeks to determine if damage or failure will occur in the resulting structural-mechanical behavior.

## **4. ANALYSES SET UP**

### **4.1. Objectives**

The stress analyses were limited to the question of whether or not the HCPB blanket box could withstand a pressurization of 8 MPa under faulted conditions. For these analyses, a half-height corner of the first wall, including stiffening grid and the back wall of the breeder box, was modeled using Solidworks 2003 and ANSYS 7.1. This portion of the breeder box can be seen in the upper left hand corner of figure 3.1.1.

### **4.2. Model Setup**

#### **4.2.1. Solid Modeling**

The model of the helium-cooled pebble bed concept was taken from work originally performed by Hermsmeyer et al [3]. Hermsmeyer provided detailed engineering drawings that were used in solid modeling and finite-element analysis for his work in [3]. These engineering drawings can be found in Appendix 1.

Using those drawings supplied by Hermsmeyer, a CAD model of the pebble bed was created using Solidworks 2003, a parametric solid modeling and assembly program. In order to implement the CAD model into the finite-element software workspace of ANSYS, the model file was saved in PARASOLID file format in Solidworks.

#### **4.2.2. ANSYS Implementation, Element Type, and Model Meshing**

The PARASOLID file of the model was imported into ANSYS for both the elastic and elasto-plastic analyses. Once the solid model was properly imported into ANSYS, the appropriate choice of element type was made. This is important because the model will be meshed entirely from the chosen element, and the overall outcome and accuracy of the solution will depend greatly on the element type, as well as the meshing options chosen.

For both elastic and elasto-plastic analyses, the element SOLID95 was used. SOLID95 can tolerate irregular shapes without much loss of accuracy, has compatible displacement shapes, and is well suited to model curved boundaries. The element is defined by 20 nodes having three degrees of freedom per node, with translations in the nodal x, y, and z directions. Also, the element may have any spatial orientation. The SOLID95 element has capabilities of plasticity, creep, stress stiffening, large deflection, and large strain, which makes SOLID95 an appropriate choice for the types of analyses needed for this project. See figure 4.2.2.1 for SOLID95 geometry and nodal configuration.

After the element type was chosen, the model was meshed. Because of the complex geometry of the model, a free mesh, rather than a mapped mesh, was performed. The free mesh was performed using the MESHTOOL, with a coarse mesh quality, which allowed for reasonable accuracy and helped in economizing computational resources.

In addition to a free mesh, one other important step was taken to economize the computational efficiency of the analyses. The original design calls for fillets of 2.5mm at sharp corners (see Appendix 1), such as between the sidewall and the back plate, among others. However, meshing such small fillets would have added enormously to the

number of elements included in the solution; thus, they were left out of the model. It is very critical to note here that sharp corners (i.e. those missing fillets) will act as extreme stress concentrations in ANSYS. Even in reality, “sharp” corners are filleted, at least on the micro- or even nanoscale. But in ANSYS, the material bulk is not made up of discrete particles or agglomerations, so sharp corners are almost atomically sharp, and thus, stress concentrations will reflect this digression from reality with unrealistically high stress results at corners.

After these steps were taken, the model was meshed, with a final element count of roughly 47,000. Figure 4.2.2.2 shows several views of the model in its fully meshed state.

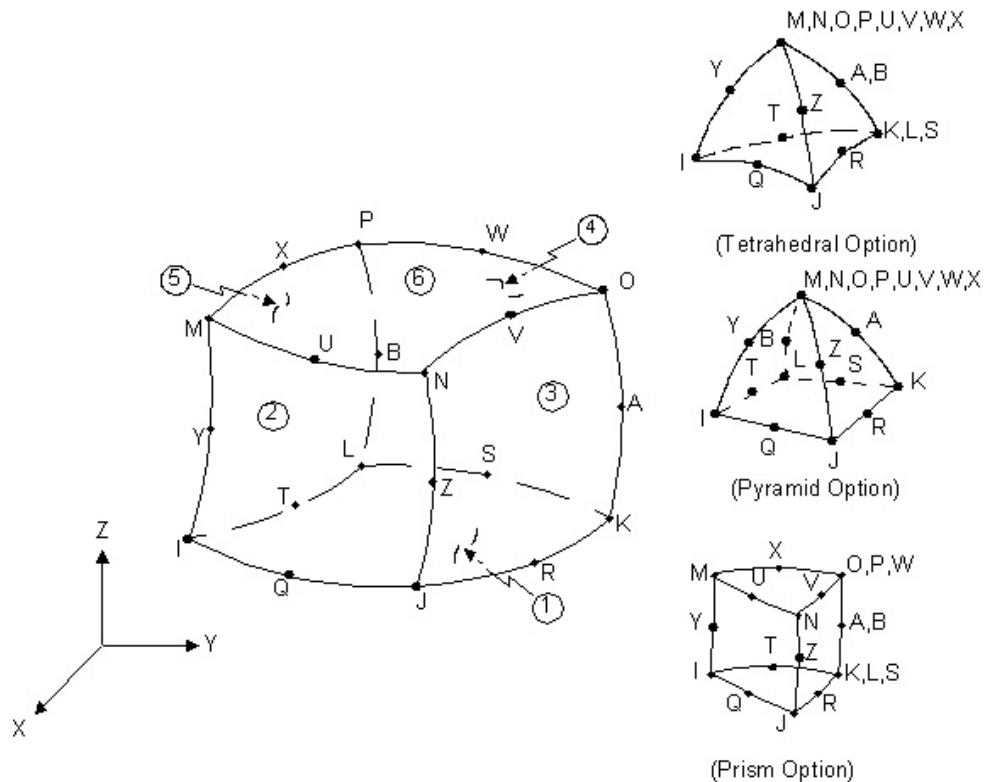


**Figure 4.2.2.1.** SOLID95 geometry and nodal configuration

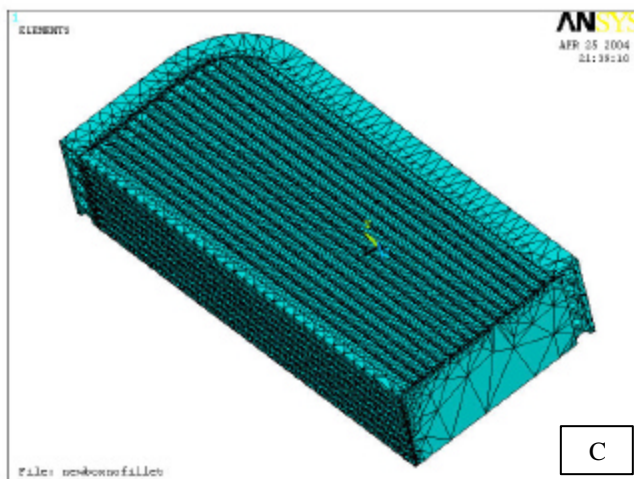
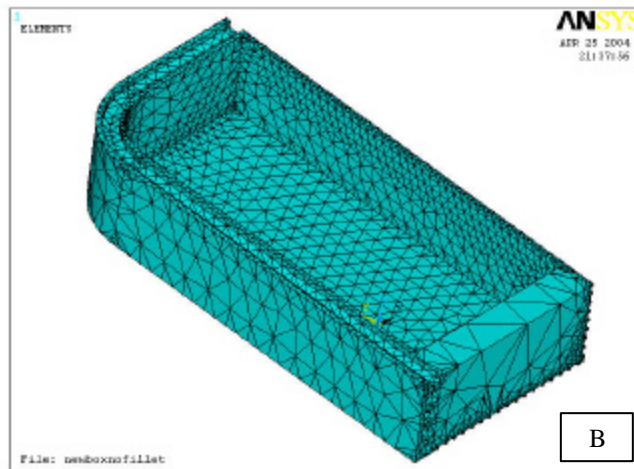
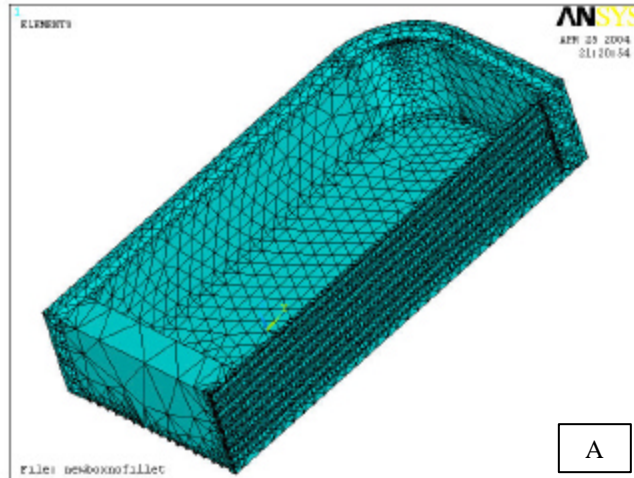


**Figure 4.2.2.2.** Completed meshed model, using brick and tetrahedral SOLID95 elements. A and B show top views of the meshed model, from two different angles. C shows the meshed model from the bottom (note the channels of the stiffening grids).

### 4.2.3. Material Models

The material assumed in the analyses was a low-activation ferritic-martensitic alloy steel known as F82H. The advantages of ferritic-martensitic alloys like F82H include low nuclear activation after disposal, the ability to withstand irradiation induced void swelling, good compatibility with liquid metal coolants, and costs [6]. For these reasons, F82H seemed to be a reasonable choice as a structural material model for the simulated fusion reactor environment in ANSYS.

Some key maximum temperatures in the blanket breeder are shown below in table 4.3.2.1. From this information, an overall model temperature was assumed to be 450°C, which allowed for a simpler material model and thus more economical computational analyses in ANSYS.

**Table 4.3.2.1.** Key maximum temperatures in the blanket. Taken from [3].

Stiffening grid	< 440°C
Cooling plate	< 540°C
First wall, at tungsten coating interface	< 550°C
Target maximum ceramic breeder	920°C
Target maximum beryllium	750°C

#### 4.2.3.1. Elastic Material Model

The material model for the purely elastic analysis involved only density and Young's modulus, and because this material model is greatly simplified, the elastic analysis may be considered as a more crude approximation of the actual structural-mechanical behavior of the material, as it does not consider the effects of plasticity past the elastic regime. The density of the steel was taken to be 7800 kg/m<sup>3</sup>. The Young's modulus was

measured from the linear portion of the true stress-strain curve obtained for F82H at 450°C; it was taken to be 181 GPa [6]. This data is summarized in table 4.3.2.1.1.

**Table 4.3.2.1.1.** Elastic material model data

<b>Young's modulus</b>	181 GPa
<b>F82H density</b>	7800 kg/m <sup>3</sup>

#### **4.2.3.2. Elasto-plastic Material Model**

The elasto-plastic material model is similar to that of the elastic model, but with the important addition of a true stress-strain curve. As with the elastic case, a Young's modulus of 181 GPa and a density of 7800 kg/m<sup>3</sup> were included in the material model. A true stress-strain curve was obtained from work done by Chiu, specifically for F82H at 450°C [6]. In his work, Chiu determined the true stress-strain curve from FORTRAN90 code that he developed using a well-known constitutive material model (Ghoniem-Matthews-Amadeo Model) derived from previous work completed by Ghoniem et al [1]. This constitutive model incorporates the effects of dislocation movement under constant stress creep testing, and Chiu extended this model to obtain local stress-strain relationships in the plastic regime [6]. Furthermore, this elasto-plastic model includes the effect of plasticity on stress and strain in the ANSYS modeling environment; therefore, it is considered a more realistic treatment of the structural-mechanical behavior of the material in the analysis. As such, results from the elasto-plastic analysis should provide a more realistic portrayal of the behavior of the material under pressure loading. The

inclusion of this true stress-strain curve completed the material model for the elasto-plastic case, and it is shown in figure 4.3.2.2.1.

#### **4.2.4. Boundary Conditions**

Because the model was taken as a half-height corner of the breeder box, we must impose symmetry boundary conditions to mirror the presence of the remainder of the box that has not been included in the modeling process. In addition to providing symmetry, these symmetry boundary conditions will anchor the box during the analyses, since the overall effect of the pressure loading will result in a net force that would otherwise cause rotation and/or translation of the model during computation, rendering an impossible solution.

Four symmetry boundary conditions were imposed on the model as follows:

- On the bottom plane surface of the model, flush with the  $z=0$  stiffening grid
- On the top plane, which represents the half-height of the model
- On the outer side plane surface, flush with the perpendicular stiffening grid
- On the back plate

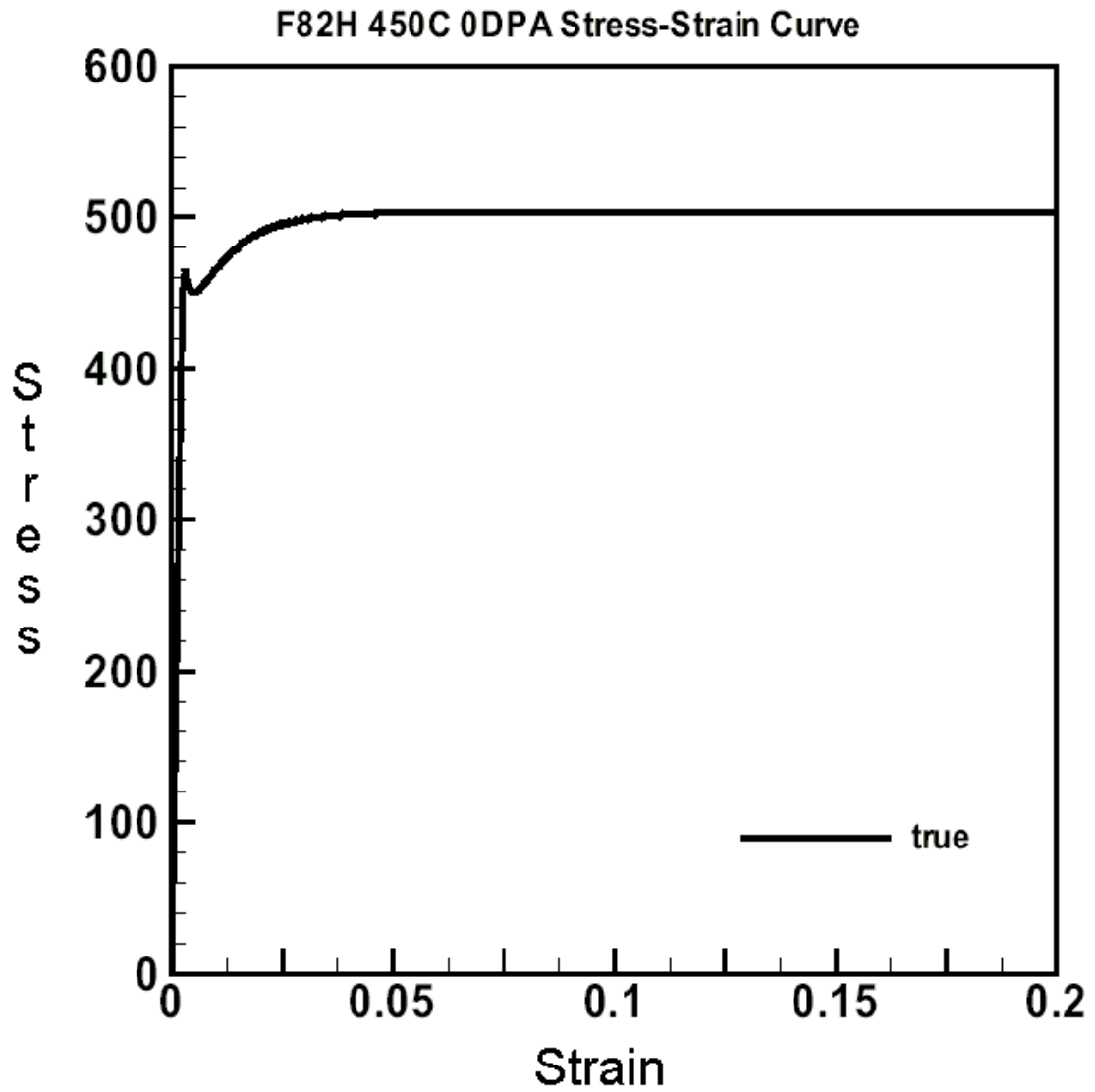


**Figure 4.3.2.2.1.** 450°C True stress-strain curve for F82H, y-axis units in MPa. Taken from [6].

#### 4.2.5. Pressure Load Application

Following the inclusion of symmetry boundary conditions, appropriate pressure loading schemes were applied to each of the three analyses. In all cases, pressure loads were applied to the same areas, that is:

- Inside the box: the inner wall of the curved first wall/sidewall boundary, the inside surface of the back plate, the floor of the box
- In the first wall/sidewall helium coolant channels
- In the channels of the bottom and side stiffening grids

Figures 4.2.5.1 and 4.2.5.2 show a more detailed view of the pressure loading scheme used for these analyses.

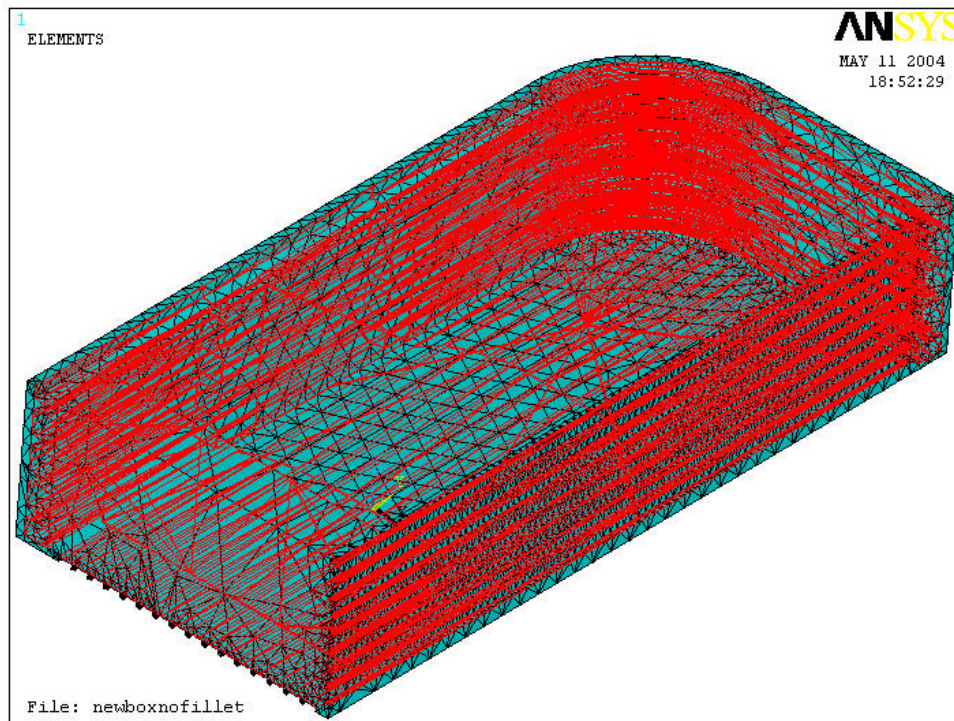


**Figure 4.2.5.1.** Pressure loading (top view). Red lines depict areas loaded with 8 MPa of pressure.

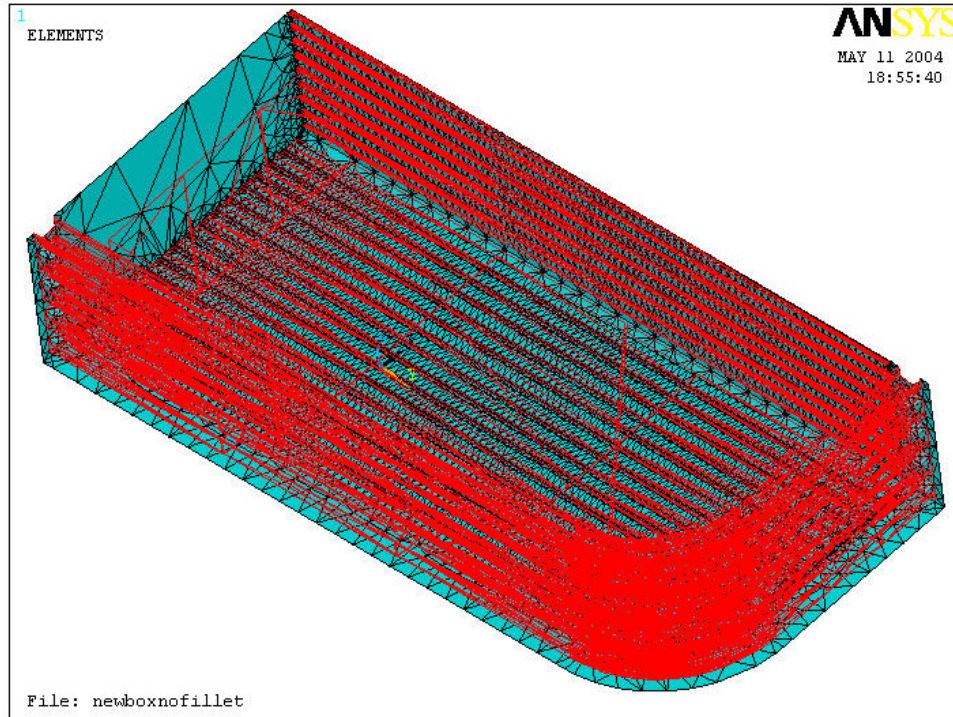


**Figure 4.2.5.2.** Pressure loading (bottom view). Red lines depict areas loaded with 8 MPa of pressure.

Both the first and second analyses were completed with a constant loading of 8 MPa on all loaded surfaces. In the third analysis, which was run using the elasto-plastic material model, the loading was broken up into steps as shown in Table 4.2.5.1, where each load step is a different constant pressure.

**Table 4.2.5.1.** Load stepping scheme for third analysis

<b>Load step number</b>	<b>Applied pressure (MPa)</b>
1	1
2	2
3	3
4	4
5	5
6	6
7	7
8	8
9	10
10	12
11	14
12	16
13	18
14	20

## **5. RESULTS & DISCUSSION**

Finally, after solid modeling and model meshing, after the appropriate material model was included, and after imposing the necessary boundary conditions and pressure loading, the ANSYS models for the three different analyses were solved. Included here are the results taken from the post-processing stage after the solutions for the analyses were completed, with appropriate discussions.

### **5.1. Elastic Analysis**

Of the three analyses, the elastic analysis is the crudest approximation of the actual structural-mechanical behavior, because it utilizes a very simple material model, where the behavior of F82H is described simply by its Young's modulus, without consideration of the effects of plasticity. As such, past the actual yield point of the material, a larger-than-normal stress should be expected, due to the lack of plasticity effects (and thus a lack of dislocation movement), which normally serves to relax some of the stresses in the material.

#### **5.1.1. Deformation Results**

Figures 5.1.1.1 through 5.1.1.4 show a variety of views of the elastic analysis results in terms of displacement (meters) due to pressure loading. It is clear from the figures that bulging occurs most significantly in the sidewall containing the helium-coolant channels. Recall that because of symmetry boundary conditions, a mirror image of the model will

be stacked on top of the box. Though the bulging appears excessive, the actual maximum value of displacement (shown in red) is 0.565mm, which is not considered significantly large. A magnification factor was used to enhance the visualization of the bulging portion of the box in ANSYS.

### **5.1.2. Von Mises Stress Results**

Figures 5.1.2.1 through 5.1.2.4 show a variety of views of the elastic analysis results in terms of von Mises stress (Pa) due to pressure loading. As would be expected, the highest stresses appear at sharp corners, where stress concentrations are particularly prone, especially in finite-element programs, such as ANSYS, where they tend to be magnified. In order to compensate for the problem of stress concentrations at corners, fillets with radius 2.5mm were originally included in the engineering drawings of the model that were provided by Hermsmeyer, but they were not included in these analyses because meshing these fillet areas would drastically increase the number of elements used. Therefore, the maximum stresses shown in the results are actually much higher than those that would normally be found in a real-world environment, since the actual structure will include fillets at the sharp corners.

The maximum stress shown for figures 5.1.2.1 and 5.1.2.2 (i.e. for the whole model) is 634 MPa (depicted in red), which occurs only at the corner between the sidewall and the back plate and nowhere else. See figure 5.1.2.5 for a magnified view of this stress concentration location. Again, the true maximum is expected to be much lower because it is considered a sharp corner by the ANSYS program. Other areas of significant stress occur at the corner between the floor of the box and the sidewall, the inside wall of the

bending portion of the sidewall, as well as in the floor of the box itself, though the values of stress in these areas are significantly lower than the value of maximum stress shown in red.

Perhaps the most significant stresses can be seen in figures 5.1.2.3 and 5.1.2.4, at the corner between the sidewall and the floor of the model, as well as on the bottom edge of the outer sidewall surface. Here, in these figures, a more realistic maximum stress exists as 315 MPa, which is well below the yield stress of the material. This analysis shows that under accidental pressurization with 8 MPa of helium-coolant gas pressure, the HCPB box will be able to maintain its structural integrity, but only if we choose to ignore the 634 MPa maximum that may be attributed to an over-emphasized stress concentration in ANSYS. Of course, because this is only an elastic analysis, and thus a crude approximation, we must beware of the accuracy of these results.

## **5.2. Elasto-plastic Analysis**

Unlike the elastic analysis, which uses only the Young's modulus of F82H to describe its structural-mechanical behavior, the elasto-plastic analysis uses the true stress-strain curve of F82H at 450°C, which provides a more realistic treatment of the material under loading. This material model considers the effects of plasticity, and thus dislocation movement, when the stress levels exceed the yield point. Therefore, past the yield point, stresses will be lower than in the purely elastic model, where plasticity effects were not included, since the movement of dislocations and plastic deformation allow for some stress relaxation in the material. However, below the yield point (i.e. in the purely elastic regime), the results from the elastic and elasto-plastic analyses should be similar.

### **5.2.1. Deformation Results**

Figures 5.2.1.1 through 5.2.1.4 show a variety of views of the elasto-plastic analysis results in terms of displacement (meters) due to pressure loading. As with the purely elastic analysis, it is clear from the figures that bulging occurs most significantly in the sidewall containing the helium-coolant channels. Though the bulging appears excessive, the actual maximum value of displacement (shown in red) is 0.564mm, which is not considered significantly large. A magnification factor was used to enhance the visualization of the bulging portion of the box in ANSYS.

### **5.2.2. Von Mises Stress Results**

Figures 5.2.2.1 through 5.2.2.4 show a variety of views of the elasto-plastic analysis results in terms of von Mises stress (Pa) due to pressure loading. Again, as would be expected, the highest stresses appear at sharp corners. As in the elastic analysis, the maximum stresses shown in the results are actually much higher than those that would normally be found in a real-world environment, since the actual structure will include fillets at the sharp corners.

The maximum stress shown for figures 5.2.2.1 and 5.2.2.2 is 547 MPa (depicted in red), which occurs only at the corner between the sidewall and the back plate and nowhere else (see figure 5.2.1.5). Again, the true maximum is expected to be much lower because it is considered an ultra-sharp corner by ANSYS. Other areas of significant stress occur at the corner between the floor of the box and the sidewall, the inside wall of the bending portion of the sidewall, as well as in the floor of the box itself, though the values of stress in these areas are significantly lower than the value of maximum stress shown in red.

Perhaps the most significant stresses can be seen in figures 5.2.2.3 and 5.2.2.4, at the corner between the sidewall and the floor of the model, as well as on the bottom edge of the outer sidewall surface. Here, in these figures, a more realistic maximum stress exists as 308 MPa—well below the yield stress of the material. This analysis shows that under accidental pressurization with 8 MPa of helium-coolant gas pressure, the HCPB box will be able to maintain its structural integrity, but only if we choose to ignore the 547 MPa maximum that may be attributed to an over-emphasized stress concentration in ANSYS. Because this is an elasto-plastic analysis, and thus a more realistic treatment of the material's structural-mechanical behavior, the accuracy of the results hold greater validity than those of the purely elastic case.

### **5.3. Elastic versus Elasto-plastic Results**

From the discussion included in sections 5.1 and 5.2, a comparison of results from the elastic analysis with those of the elasto-plastic analysis gives an insight into the similarities and differences between the two material models and their results. If we consider a pressure loading scenario where the yield point of the material is not exceeded at any point, then we would expect to see similar deformation and von Mises stress behavior. However, should any portion of the model exceed the yield point, we will see a higher stress in the elastic case than in the elasto-plastic case, as described earlier.

From the results of both the elastic and elasto-plastic case, we see that only the corner between the sidewall and the back plate (figure 5.2.1.5) experiences a stress—that is, the maximum stress, in red—that exceeds the yield point (see F82H true stress-strain curve, figure 4.3.2.2.1). For the elastic case, this maximum stress is 634 MPa, while for the

elasto-plastic case, the maximum stress is 547 MPa. Thus, we can see that the elasto-plastic material model properly includes the stress-relaxing effects of plasticity and dislocation movement to reduce the stress significantly when compared to the elastic model.

But, recall that this maximum stress occurs at an over-emphasized stress concentration, where a fillet has not been included in the ANSYS environment. Since the actual HCPB box will include fillets at sharp corners, the stress concentration will be greatly reduced. Therefore, in reality, stresses may not exceed the yield point, in which case the behavior of the entire structure will be elastic. This case is illustrated by comparing figures 5.1.2.3 and 5.1.2.4 (elastic analysis) to figures 5.2.2.3 and 5.2.2.4 (elasto-plastic analysis), all of which are sectioned views of the model that exclude the stress concentration that exceeds the yield stress at the corner between the back plate and the sidewall. These figures show maximum stresses at the corner between the sidewall and the floor of the box, as well as on the bottom edge of the outer sidewall surface. In the elastic case, the maximum stress (see figures 5.1.2.3 and 5.1.2.4 in red) is 315 MPa. Similarly for the elasto-plastic case, the maximum stress (see figures 5.2.2.3 and 5.2.2.4 in red) is 308 MPa. We can see here that since the stresses are below the yield stress of the material, the stress behavior of the elastic and elasto-plastic analyses are, for all intents and purposes, virtually the same. This also applies to deformation results between the two different analyses. The maximum displacement in the elastic case was 0.565mm, while in the elasto-plastic case the maximum was 0.564mm, which is almost exactly the same value. Both occur at the bulge in the sidewall.

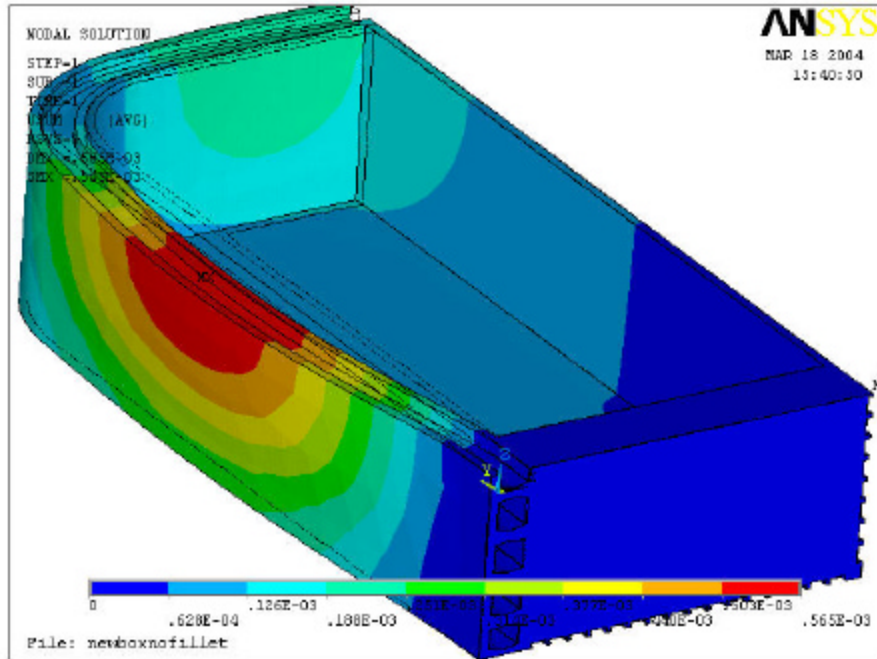


**Figure 5.1.1.1.** Elastic analysis displacement (top view), shown in meters. The outline of the undeformed shape is shown as black dotted lines.

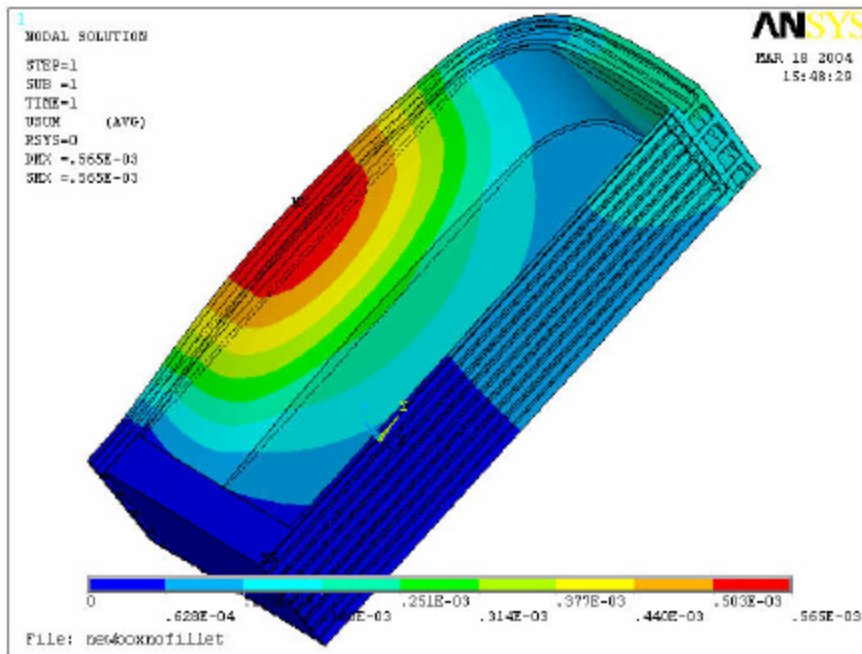


**Figure 5.1.1.2.** Elastic analysis displacement (top view), shown in meters. The outline of the undeformed shape is shown as black dotted lines.

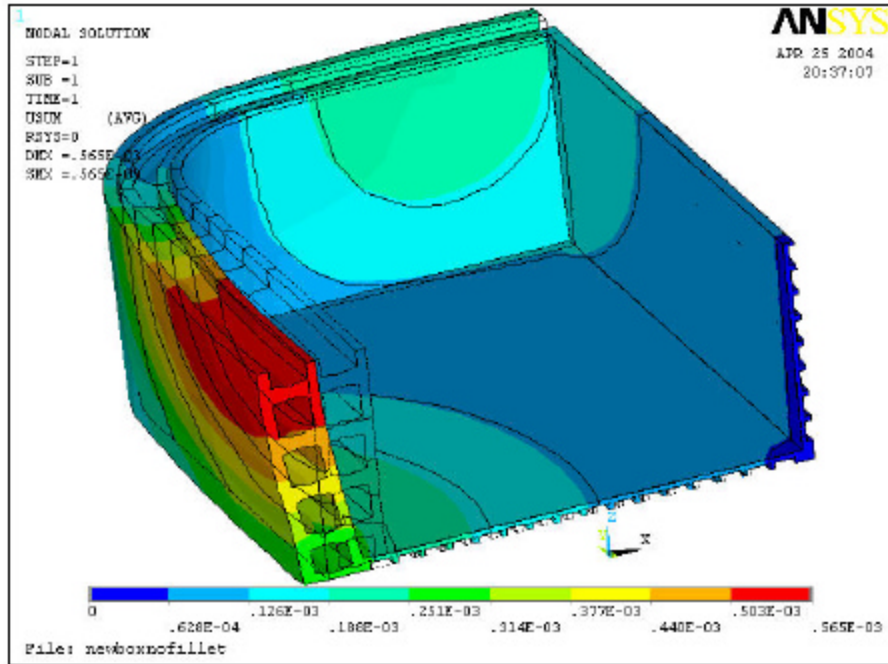


**Figure 5.1.1.3.** Elastic analysis displacement (isometric/section view), shown in meters. The outline of the undeformed shape is shown as black dotted lines.

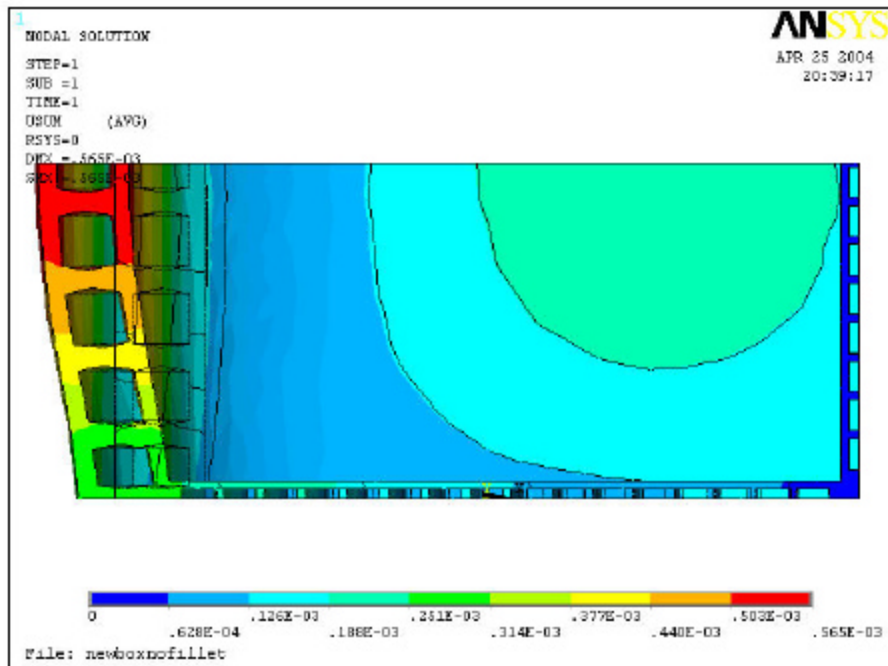


**Figure 5.1.1.4.** Elastic analysis displacement (section view), shown in meters. The outline of the undeformed shape is shown as black dotted lines.

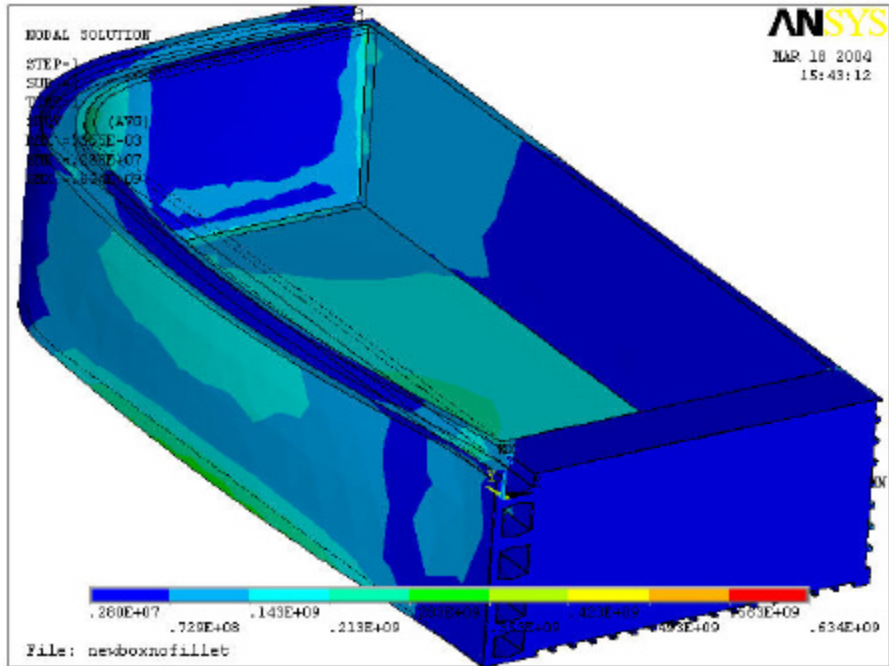


**Figure 5.1.2.1.** Elastic analysis von Mises stress (top view), shown in Pascals. The outline of the undeformed shape is shown as black dotted lines.

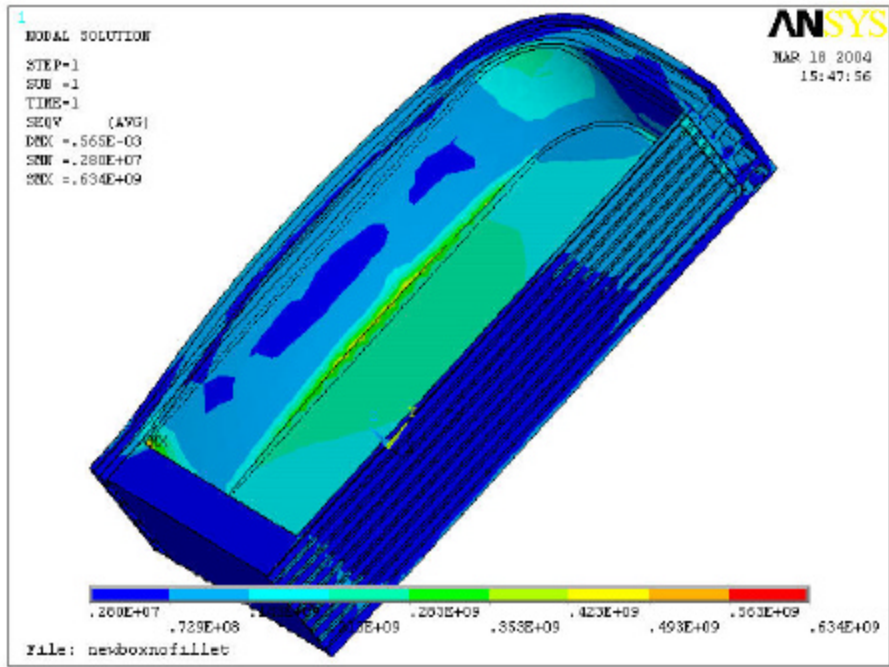


**Figure 5.1.2.2.** Elastic analysis von Mises stress (top view), shown in Pascals. The outline of the undeformed shape is shown as black dotted lines.

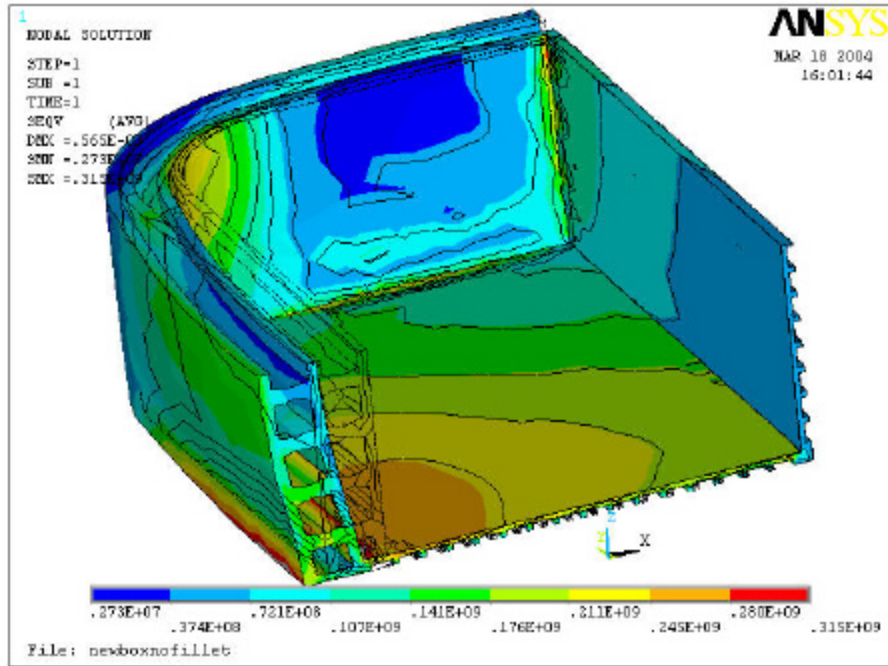


**Figure 5.1.2.3.** Elastic analysis von Mises stress (isometric/section view), shown in Pascals. The outline of the undeformed shape is shown as black dotted lines.

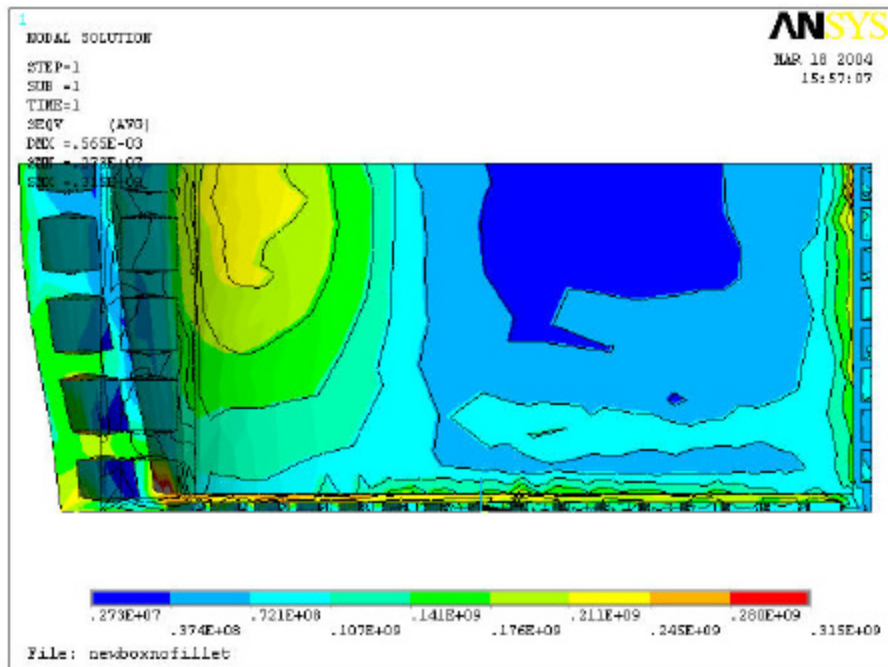


**Figure 5.1.2.4.** Elastic analysis von Mises stress (section view), shown in Pascals. The outline of the undeformed shape is shown as black dotted lines.

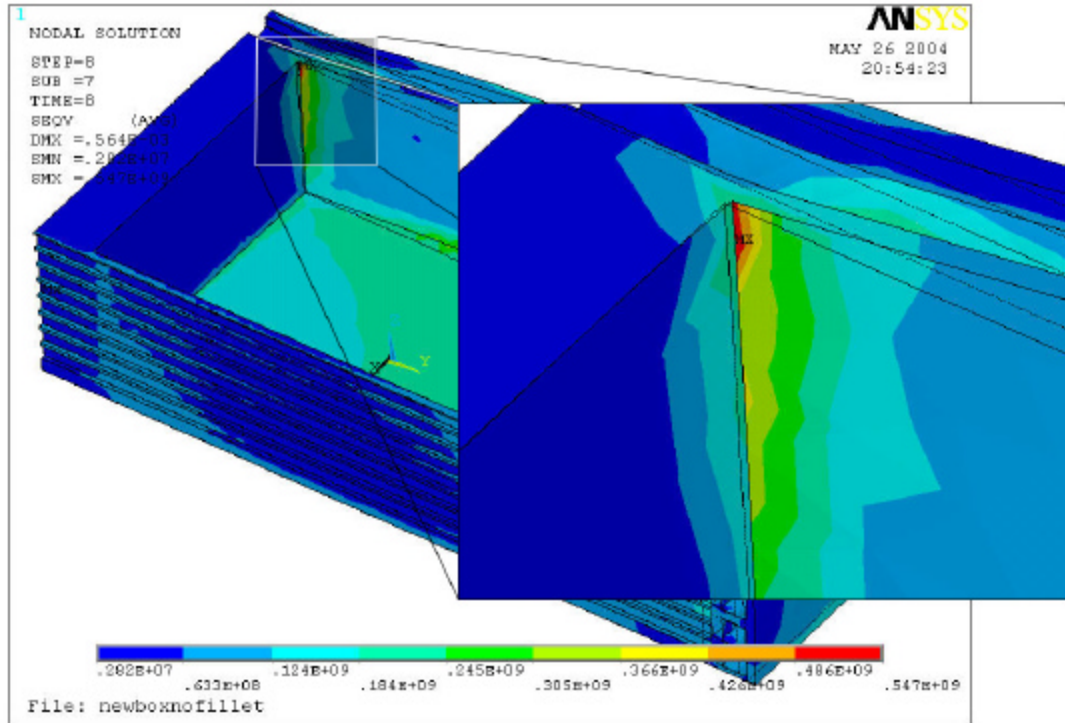


**Figure 5.1.2.5.** Magnified view of maximum von Mises stress location.

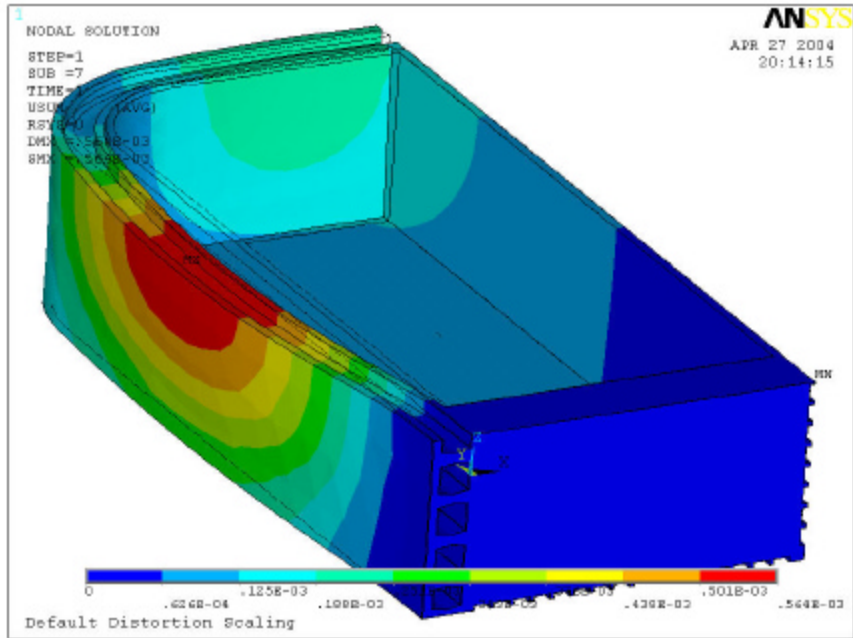


**Figure 5.2.1.1.** Elasto-plastic analysis displacement (top view), shown in meters. The outline of the undeformed shape is shown as black dotted lines.

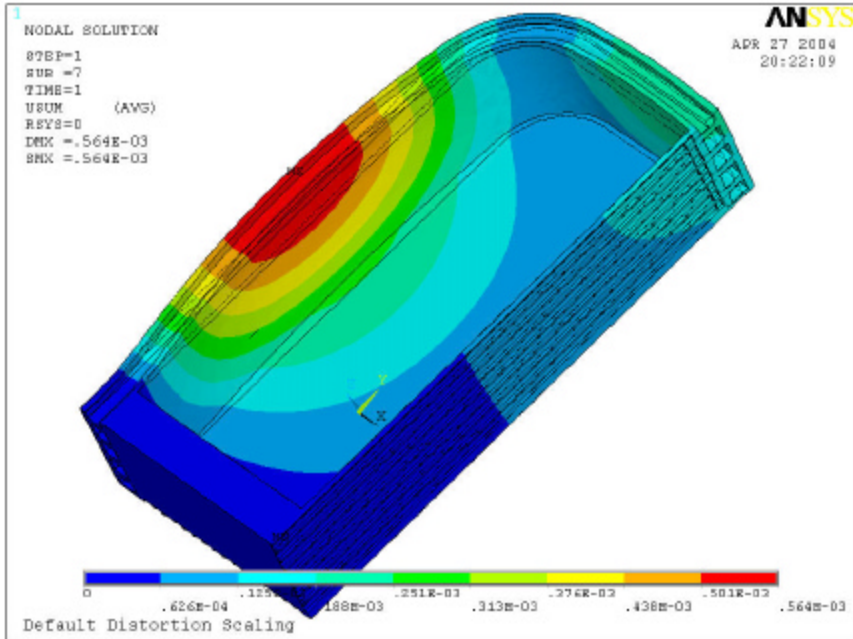


**Figure 5.2.1.2.** Elasto-plastic analysis displacement (top view), shown in meters. The outline of the undeformed shape is shown as black dotted lines.

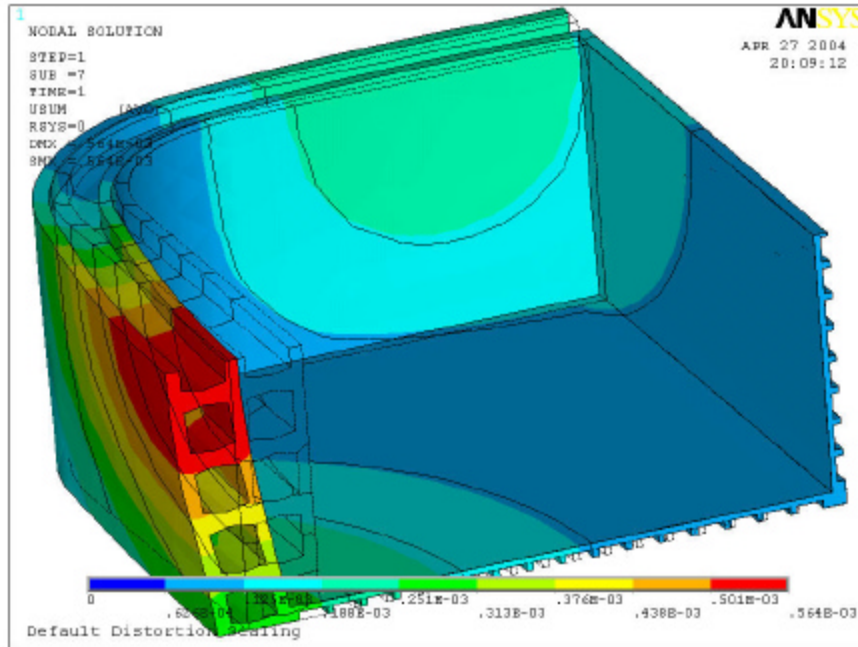


**Figure 5.2.1.3.** Elasto-plastic analysis displacement (isometric/section view), shown in meters. The outline of the undeformed shape is shown as black dotted lines.

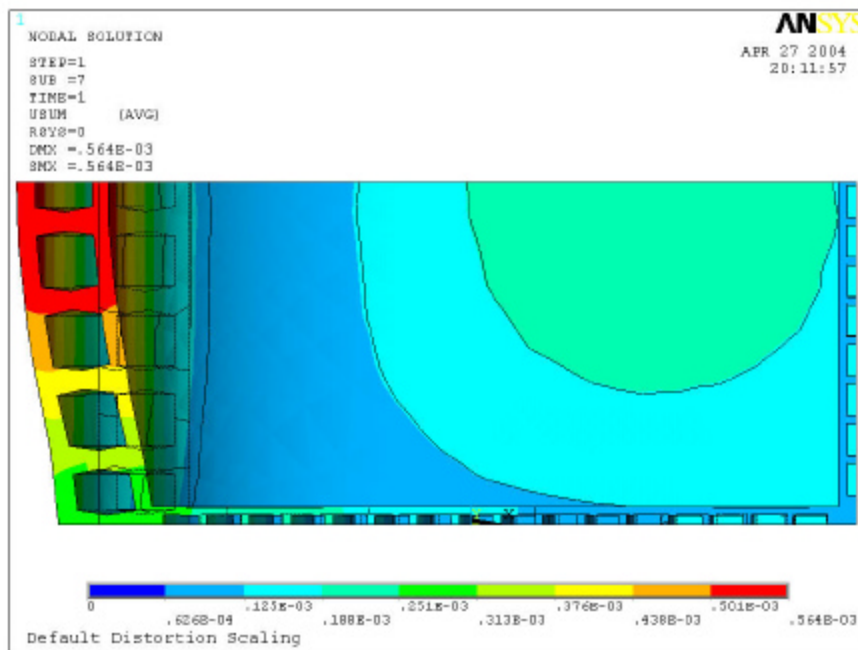


**Figure 5.2.1.4.** Elasto-plastic analysis displacement (section view), shown in meters. The outline of the undeformed shape is shown as black dotted lines.

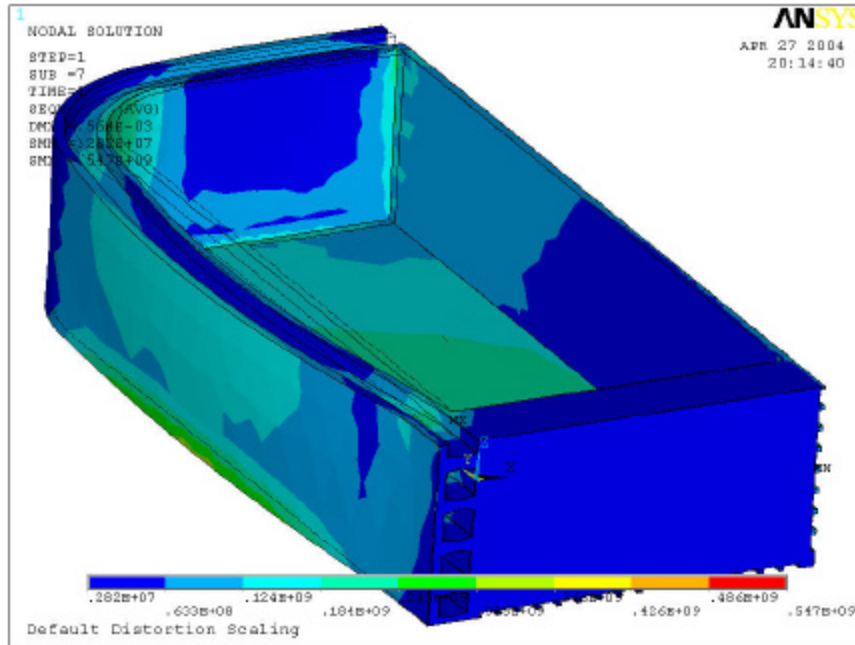


**Figure 5.2.2.1.** Elasto-plastic analysis von Mises stress (top view), shown in Pascals. The outline of the undeformed shape is shown as black dotted lines.

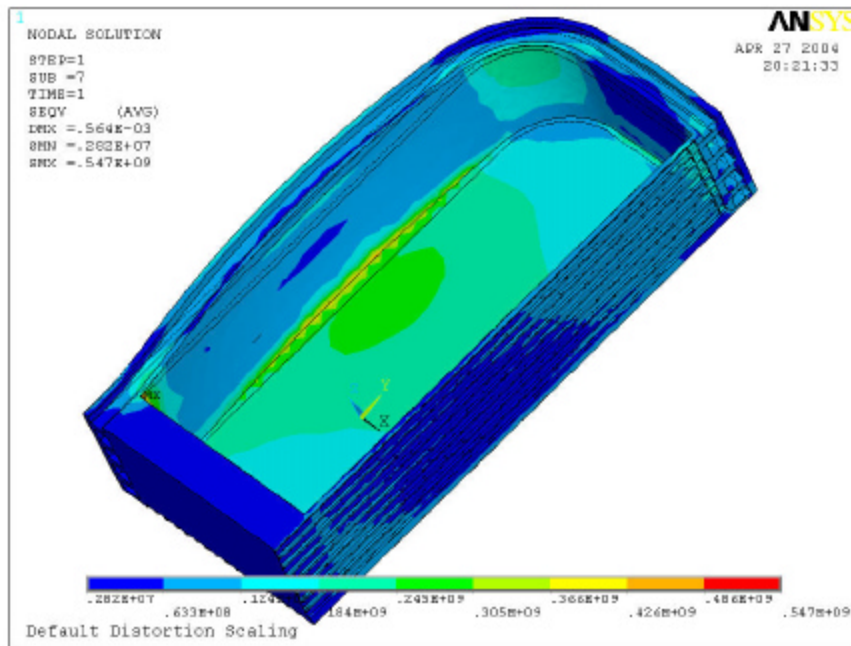


**Figure 5.2.2.2.** Elasto-plastic analysis von Mises stress (top view), shown in Pascals. The outline of the undeformed shape is shown as black dotted lines.

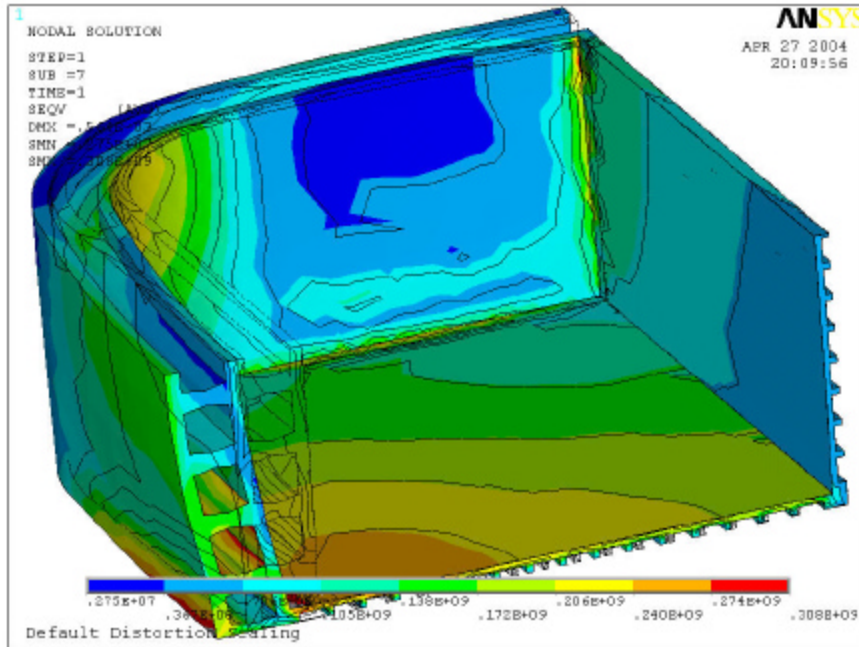


**Figure 5.2.2.3.** Elasto-plastic analysis von Mises stress (isometric/section view), shown in Pascals. The outline of the undeformed shape is shown as black dotted lines.

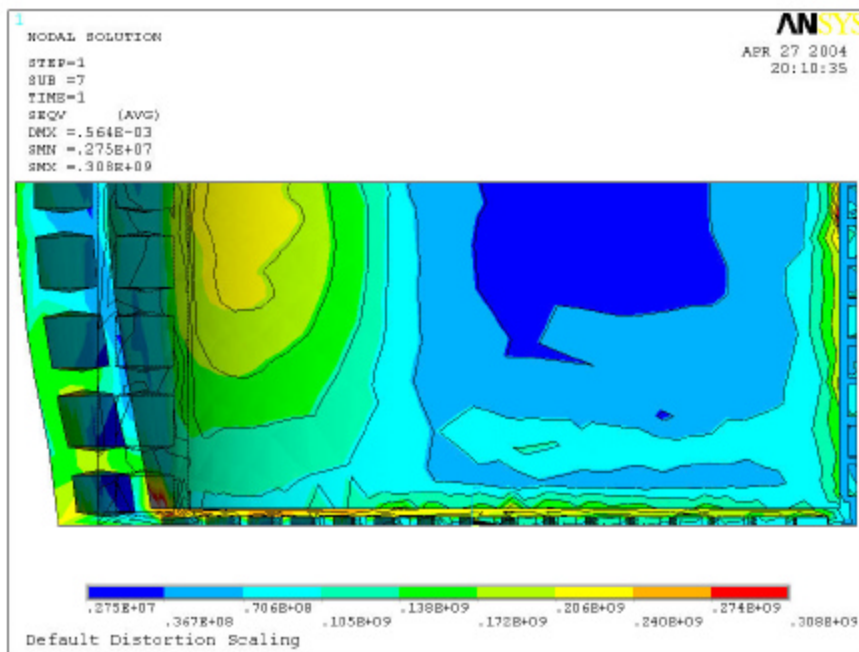


**Figure 5.2.2.4.** Elasto-plastic analysis von Mises stress (section view), shown in Pascals. The outline of the undeformed shape is shown as black dotted lines.

#### **5.4. Step Loading Results**

The final analysis was completed using a pressure loading scheme that stepped incrementally (see table 4.2.5.1). The loading scheme greatly exceeds the faulted box pressurization level of 8 MPa, up to 20 MPa. The elasto-plastic material model was used for this analysis to account for plasticity effects past the yield point. After the solution was completed, data for resultant maximum strains, stresses, and displacements were gathered for each load step. These data were then plotted versus load increments. Each data point in the following graphs represents a load step that was solved in ANSYS. Figure 5.4.1 shows maximum nodal displacement (in meters). Figure 5.4.2 shows maximum nodal strain. Figure 5.4.3 shows maximum stress (in Pa). All three graphs are functions of load step pressure (in MPa). Figures 5.4.4, 5.4.5, and 5.4.6 show contour plots of displacement, strain, and von Mises stress, respectively, as pressure is increased. Each of these three figures shows six contour plots that correspond to six selected pressures in MPa: 3, 5, 8, 12, 16, and 20. Note that the data represented by these figures do not coincide with the same node or point location, since maximums for various types of behavior will occur at different areas and nodes, as is the case here.

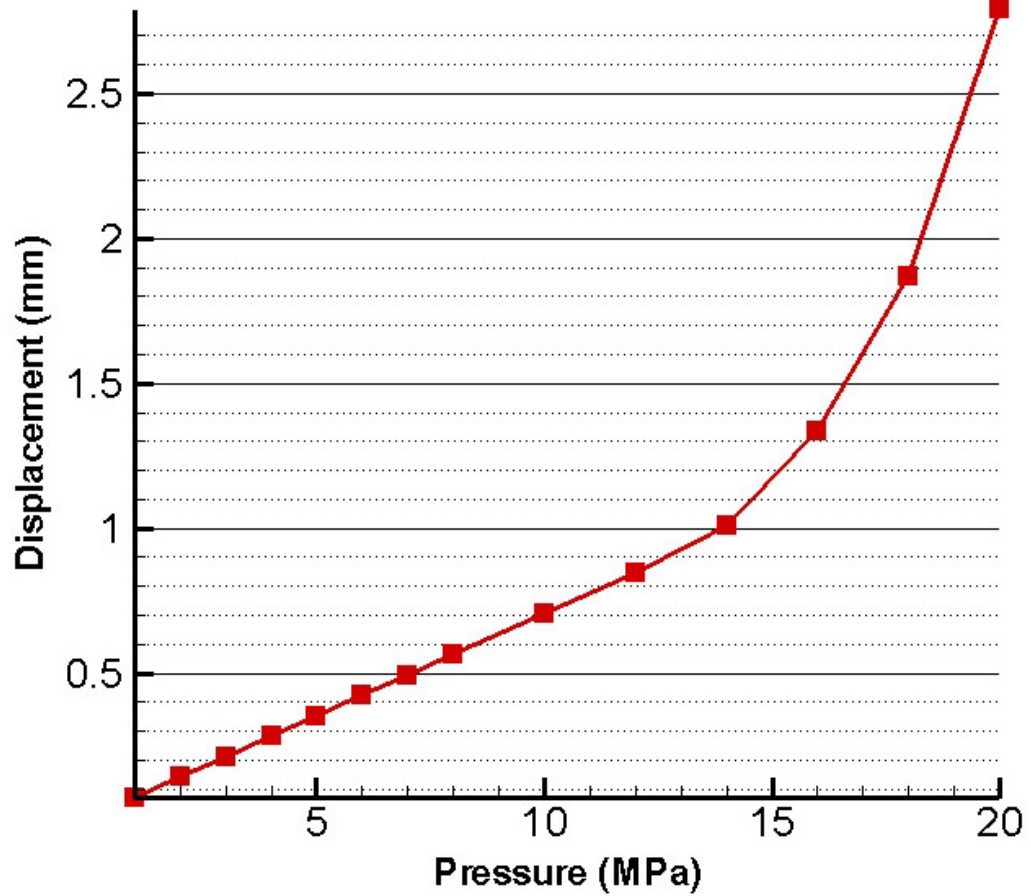


**Figure 5.4.1.** Evolution of maximum nodal displacement as a function of helium coolant pressure.

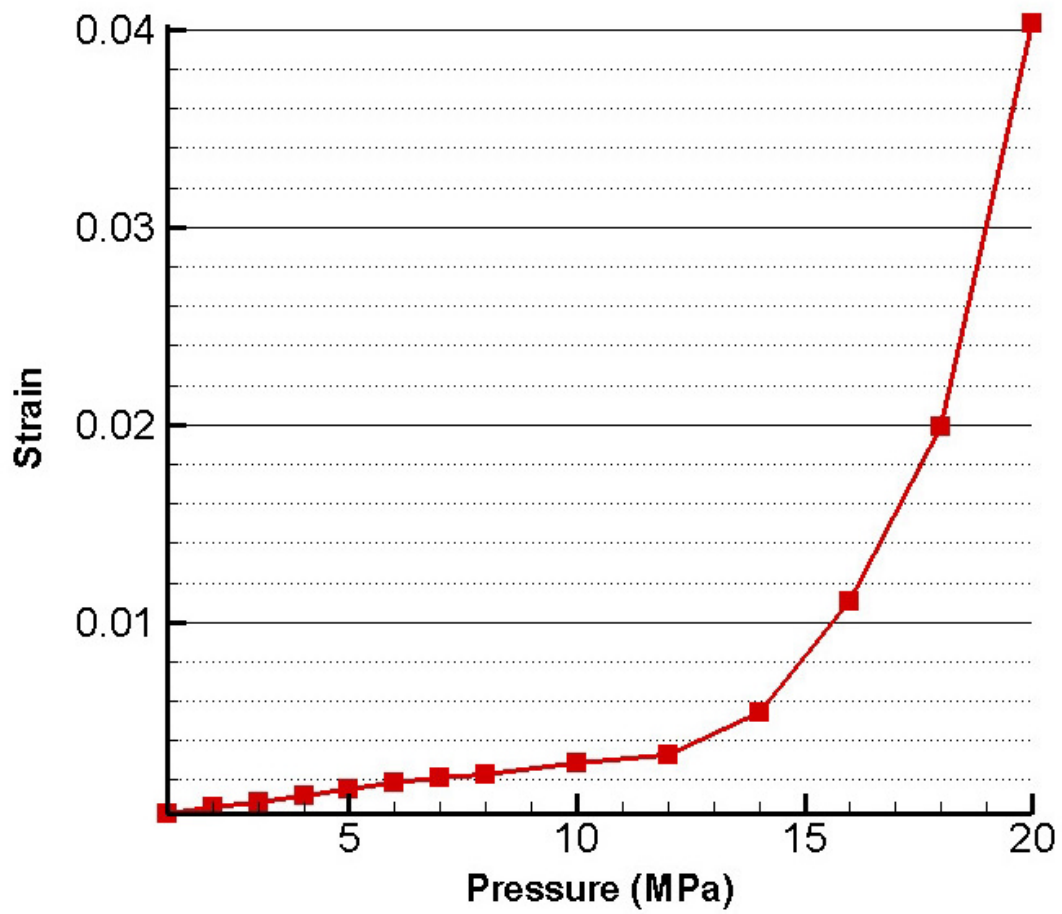


**Figure 5.4.2.** Evolution of maximum nodal strain as a function of helium coolant pressure.

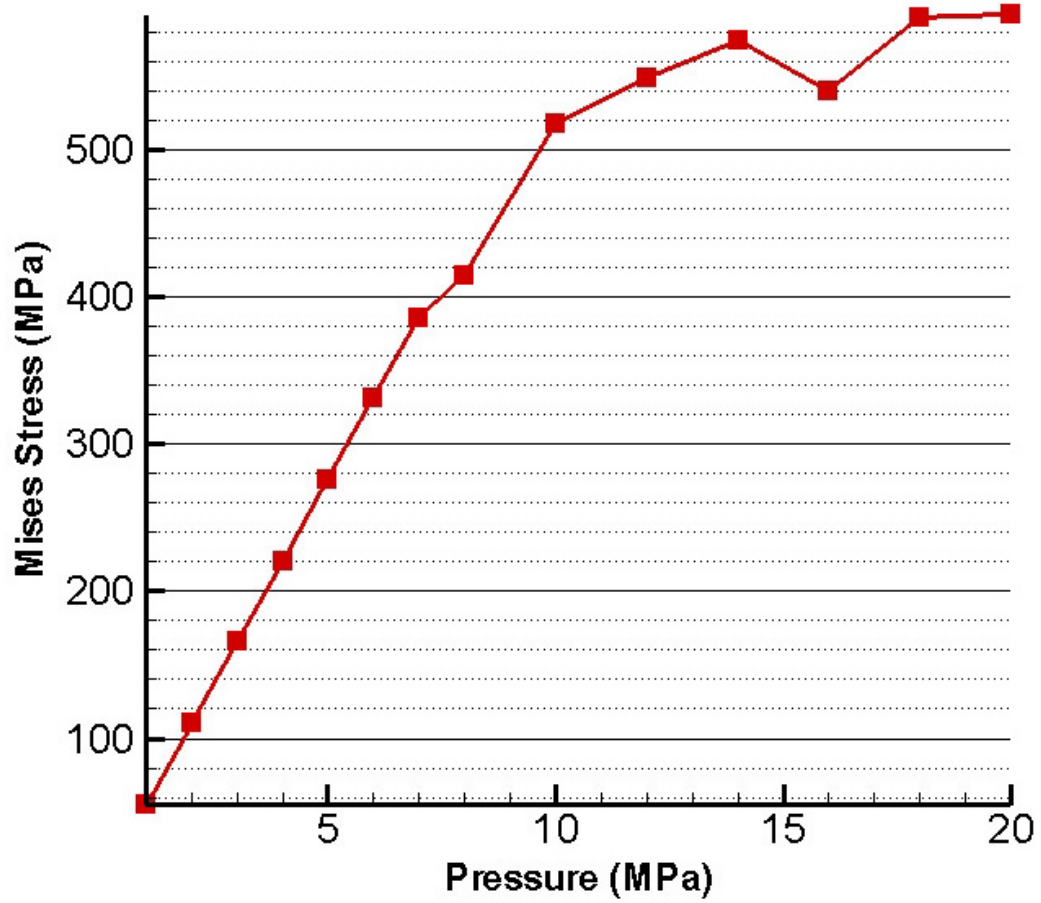


**Figure 5.4.3.** Evolution of maximum nodal von Mises stress as a function of helium coolant pressure.

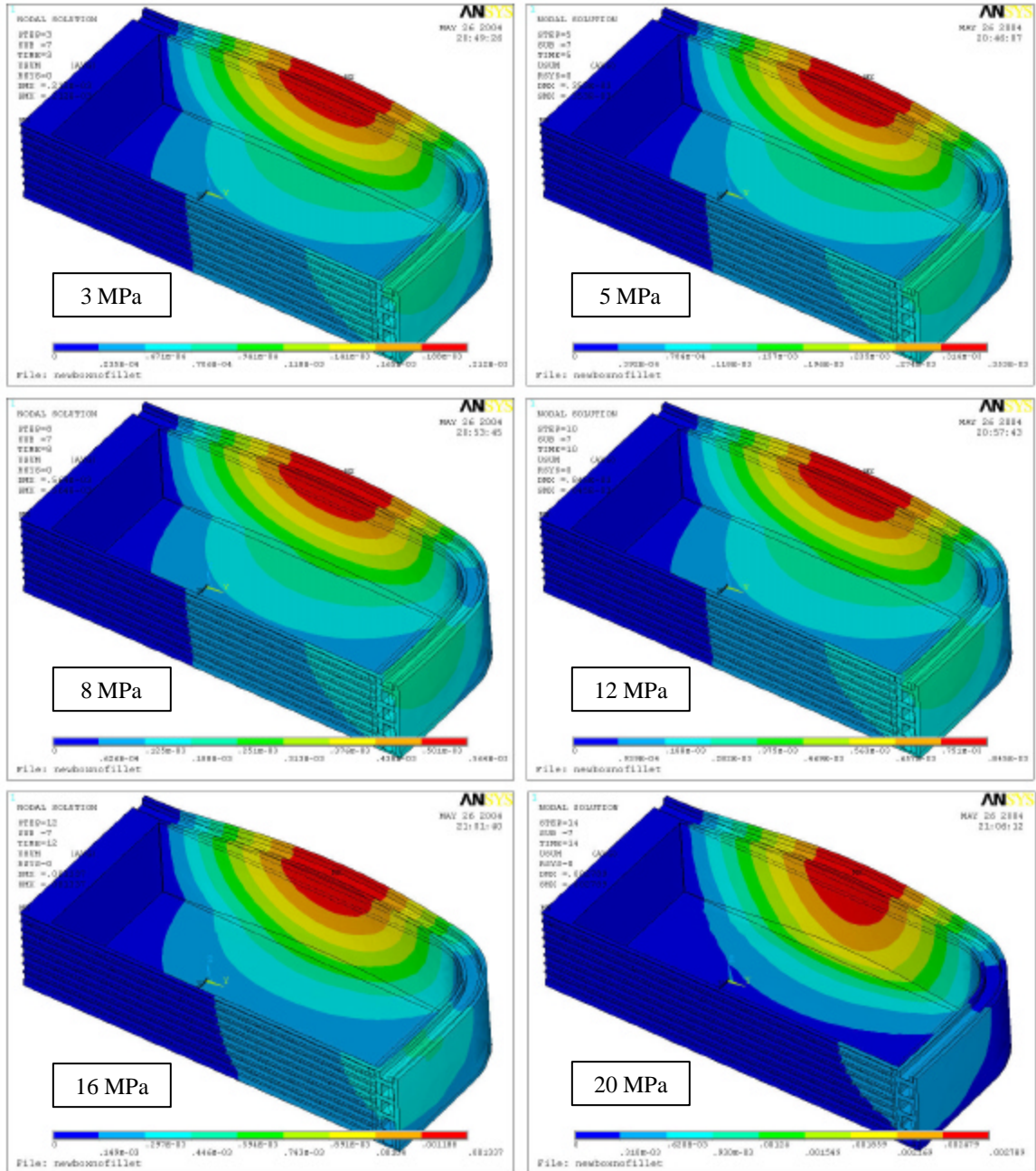


**Figure 5.4.4.** Evolution of HCPB box displacement (m) with increasing pressure.

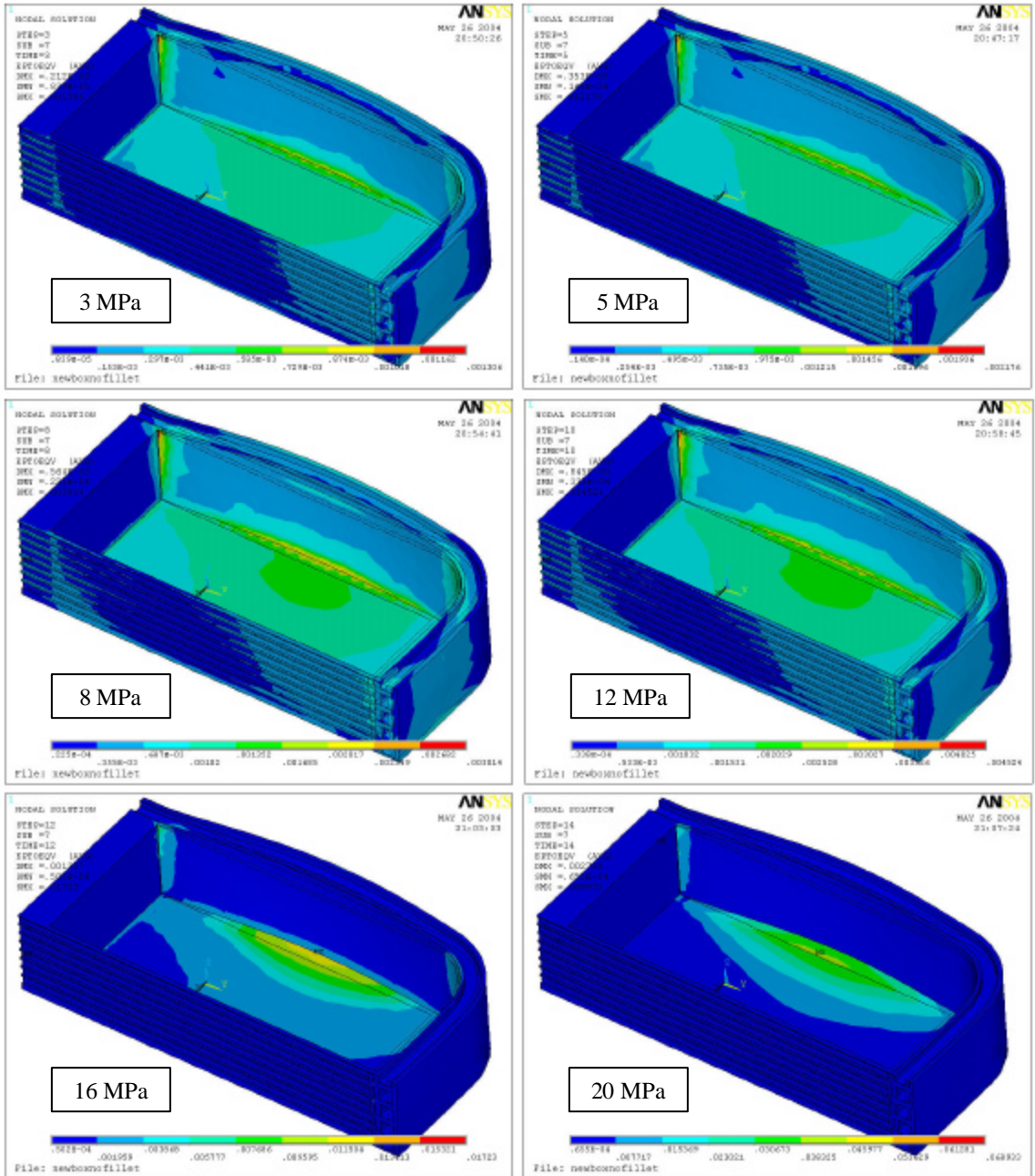


**Figure 5.4.5.** Evolution of HCPB box strain with increasing pressure.

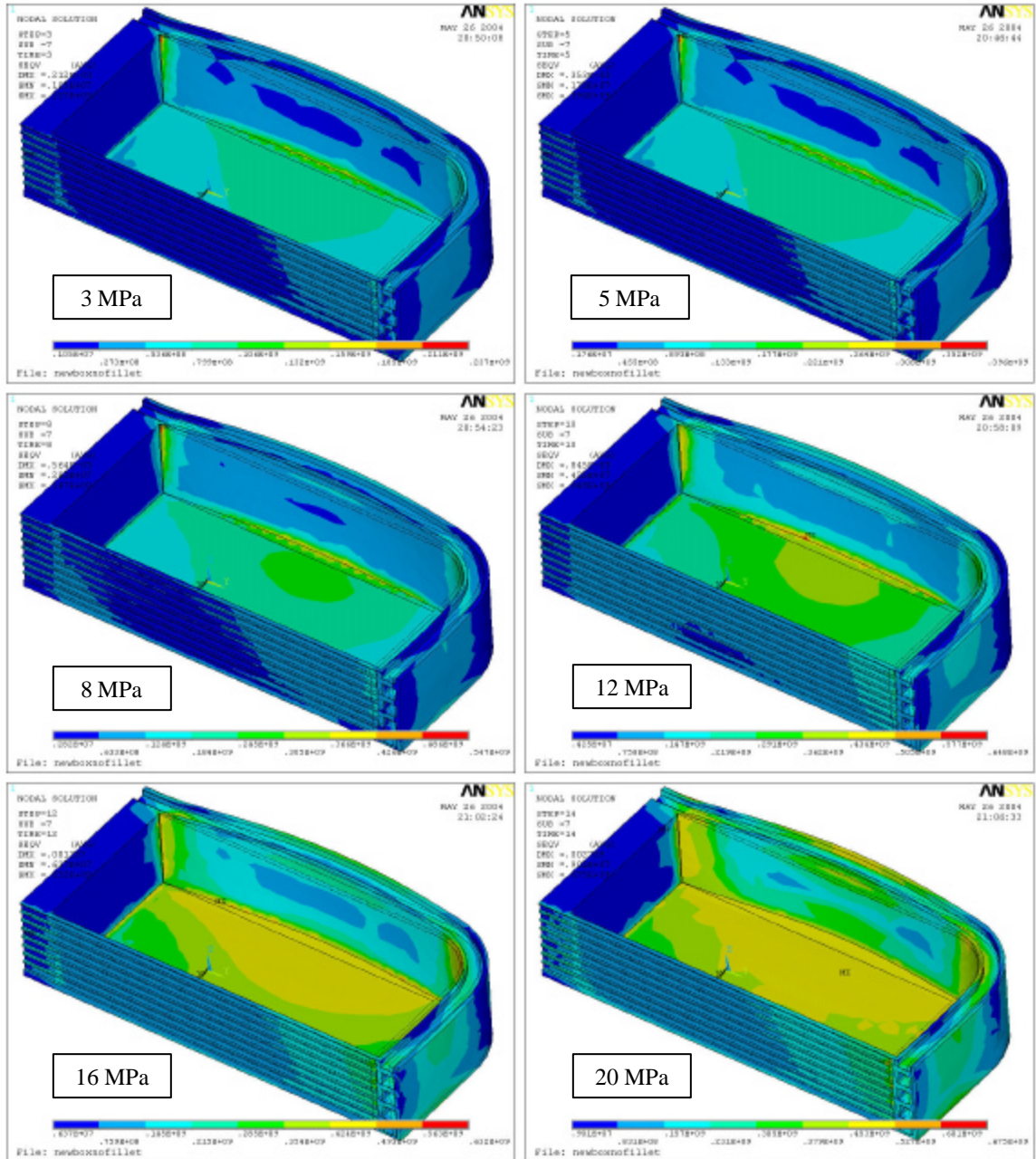


**Figure 5.4.6.** Evolution of HCPB box von Mises stress (MPa) with increasing pressure.

### **5.4.1. Displacement and Strain Results**

As the pressure was increased from 1 MPa to 12 MPa, the displacement and strain responded linearly, as shown in figures 5.4.1 and 5.4.2. Past 12 MPa, the slopes of the displacement and strain curves increase with each load step, which shows that the material is beginning to deform plastically, where the structural-mechanical behavior of the material is no longer elastic. Thus, the elastic limit of the displacement and strain behavior appears to be around 12 MPa. Therefore, we may expect the HCPB box to withstand the resultant deformation and strain without permanent plastic deformation, with an upper limit of plastic deformation that is significantly higher than the helium coolant pressure of 8 MPa. The evolution of displacement and strain are also shown in contour plots included in figures 5.4.4 and 5.4.5.

### **5.4.2. Stress Results**

As the pressure is increased from 1 MPa to 10 MPa, the von Mises stress responds fairly linearly, as shown in figure 5.4.3. Past 10 MPa, the slope of the von Mises stress curve generally decreases with each load step up to about 20 MPa, where it is expected that the slope of the curve will flatten out past this point, should the material avoid failure at higher pressures. This behavior past 10 MPa shows that the material is beginning to deform plastically, where the structural-mechanical behavior of the material is no longer elastic. Thus, the elastic limit of the stress behavior appears to be around 10 MPa. Therefore, the HCPB concept will behave elastically without permanent plastic damage or failure up to 10 MPa, which is significantly greater than the coolant pressure of 8 MPa. The evolution of von Mises stress is shown in contour plots included in figure 5.4.6.

Finally, note in figure 5.4.3 the anomalous data point at a pressure of 16 MPa, where the curve experiences a significant and unexpected drop in von Mises stress, only to return to its original behavior in the subsequent data point. This anomaly is believed to have resulted from one of two causes. Firstly, it is possible that at this pressure of 16 MPa, the material experienced a plastic instability due to a “kink” in the true stress-strain curve imported into the ANSYS model (see figure 4.3.2.2.1). Secondly, since the maximum stress likely occurs in a corner or at other sharp edges (see figure 5.1.2.5 and section 5.1.2) where stress concentrations are exaggerated in ANSYS, it is possible that the maximum stress results will reflect the instabilities and inaccuracies of the ANSYS program at such sharp corners, particularly in the plastic regime. Simply put, this translates to an error factor in ANSYS that may need to be considered in evaluating the results in figure 5.4.3.

## 6. SUMMARY & CONCLUSIONS

The modeling and finite-element analyses results presented in this project seek to determine whether or not the helium-cooled pebble blanket box concept will be able to withstand a box pressurization to the level of the helium coolant pressure of 8 MPa in the case of an internal leak.

In this work, three different analyses were performed. The first involved the assumption that elastic material properties applied. The second used a more rigorous modeling approach, where elasto-plastic material properties were assumed. The third analysis also used elasto-plastic material properties, with the addition of stepped pressure loading, to examine structural-mechanical behavior past the faulted box pressure of 8 MPa. In all analyses, displacements and stresses were computed and plotted. In the third analysis, results for strain were also computed and plotted, in addition to displacement and stress. Based on these results the following conclusions can be drawn.

1. A true stress-strain curve for F82H at 450°C, obtain from Chiu, was successfully implemented into ANSYS for the elasto-plastic material properties.
2. From contour plot data, the most significant deformation due to box pressurization will occur in the sidewall portion of the box. The maximum displacement under a pressure of 8 MPa was small—roughly 0.5mm—and should

not be considered significant. The displacement results were the same for the elastic and elasto-plastic analyses.

3. Maximum von Mises stress for the elastic case was found to be 634 MPa, which is well above the elastic limit of the material. Based on this result alone one may conclude that the material will experience failure or at least permanent plastic damage. However, the location of this stress maximum was determined to be at the corner between the sidewall and the back plate (figure 5.1.2.5), and as such, it can be considered a stress concentration. Furthermore, because ANSYS models such corners as extremely sharp edges, the stress concentration will be greatly magnified. Hence, the true maximum stress is expected to be much lower than 634 MPa, in which case the maximum given by ANSYS may be disregarded as unrealistically high. This leads us to look at other areas of significant stress in the HCPB box where stress concentrations are not as exaggerated. Upon examination of the contour plots for stress, we see that a more reasonable von Mises stress of 315 MPa exists between the floor of the box and the sidewall, which is well below the yield stress of the material. If we ignore the stress concentration mentioned earlier, we may instead take the 315 MPa result as final, meaning that the HCPB box will behave elastically under a pressure load of 8 MPa, without damage or failure.

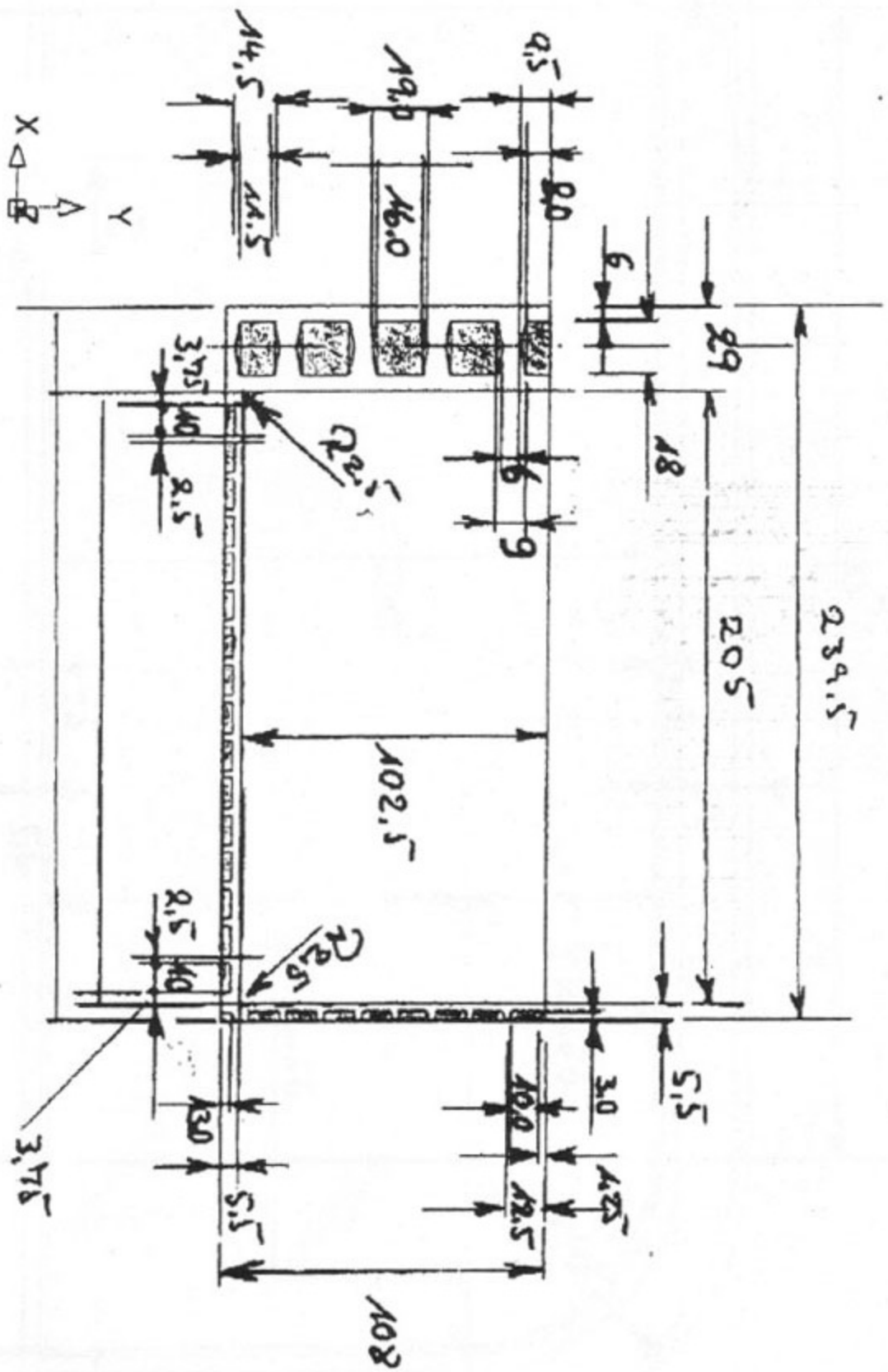
4. Maximum von Mises stress for the elasto-plastic case was found to be 547 MPa, which, as with the elastic case, is well above the elastic limit of the material. This result is significantly lower than the maximum von Mises stress of the elastic case, since the elasto-plastic material properties consider the effect of plasticity on the structural-mechanical behavior of F82H, where plastic deformation allows for stress relaxation, unlike the elastic case. However, this result can be considered unrealistically high for the same reasons stated in conclusion 3 above—that reason being the exaggerated stress concentration at the corner between the sidewall and the back plate. When considering other areas of significant stress concentrations, a more realistic maximum of 308 MPa was found in the area between the floor of the box and the sidewall, similar to the elastic case. When we disregard the exaggerated stress concentration of 547 MPa and take the 308 MPa result as final, we may conclude that the HCPB box will behave elastically under a pressure load of 8 MPa, without damage or failure.
  
5. If we choose to ignore the exaggerated stress concentrations in the elastic and elasto-plastic analyses, it becomes apparent that the stress results for both cases are virtually the same. Furthermore, the displacement behavior is similar between the elastic and elasto-plastic cases. Hence, the elastic analysis can be considered a reasonable approximation of the elasto-plastic analysis, but only when the structural-mechanical behavior of both analyses remain in the elastic regime, as is assumed in this project with a box pressure of 8 MPa.

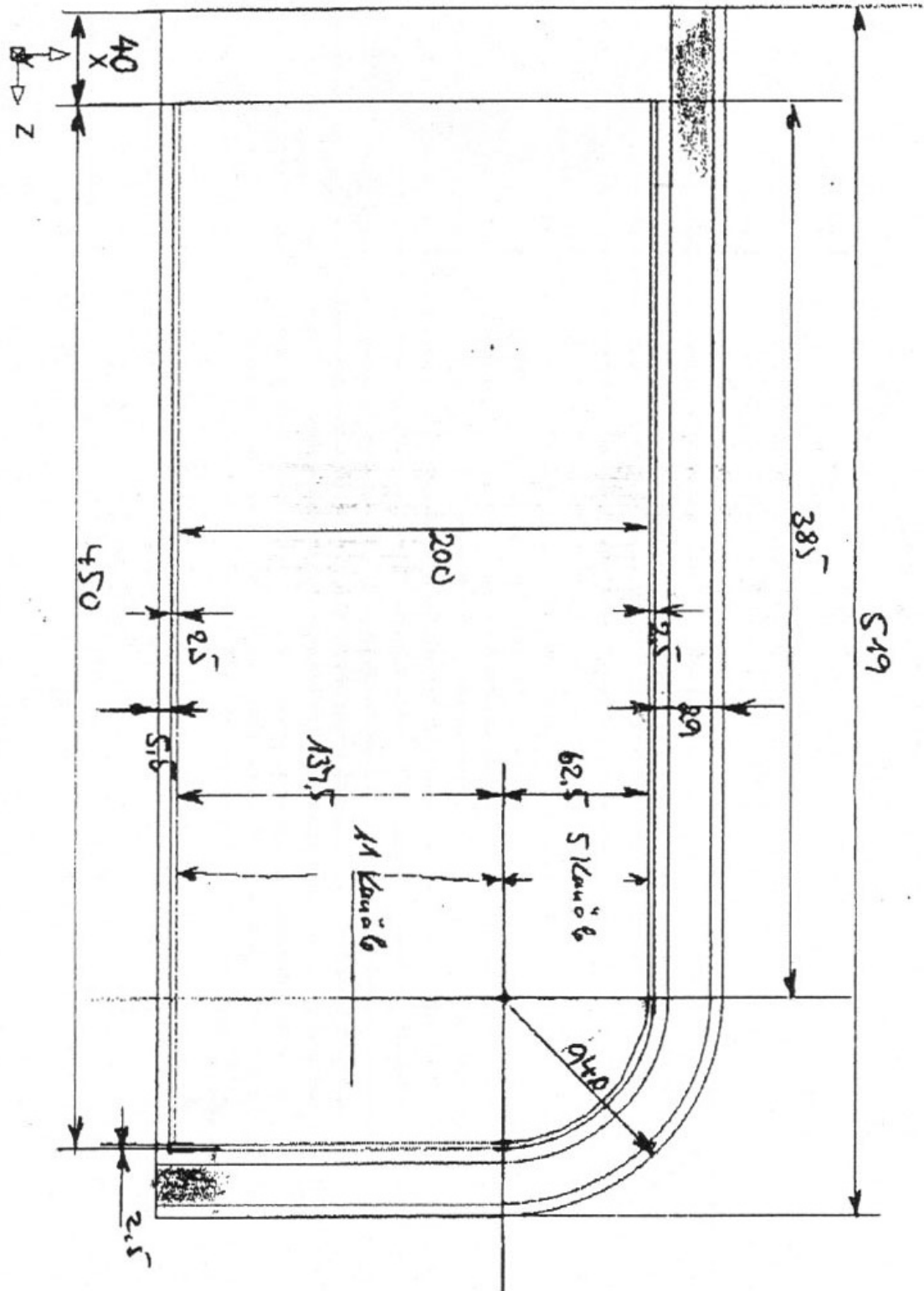
6. As the pressure was increased from 1 MPa to 12 MPa, the displacement and strain responded linearly in the stepped pressure load analysis. Past 12 MPa, the material deforms and strains plastically, as shown in the nonlinear behavior of the data. Thus, the elastic limit of the displacement and strain behavior appears to be around 12 MPa.
  
7. As the pressure is increased from 1 MPa to 10 MPa, the von Mises stress responds fairly linearly for the stepped pressure load analysis. Past 10 MPa, the slope of the von Mises stress curve generally decreases with each load step up to about 20 MPa, where it is expected that the slope of the curve will flatten out past 20 MPa, should the material avoid failure at higher pressures. Thus, the elastic limit of the stress behavior appears to be around 10 MPa. Hence, we may expect the HCPB box to withstand the resultant stress up to about 10 MPa without permanent plastic deformation damage, with an upper limit of plastic deformation that is significantly higher than the helium coolant pressure of 8 MPa.
  
8. The anomalous data point in figure 5.4.3 is believed to have resulted from one of two causes. Firstly, it is possible that at a pressure of 16 MPa, the material experienced a plastic instability due to a “kink” in the true stress-strain curve imported into the ANSYS model (figure 4.3.2.2.1). Secondly, since the maximum stress likely occurs in a corner or at other sharp edges (figure 5.1.2.5,

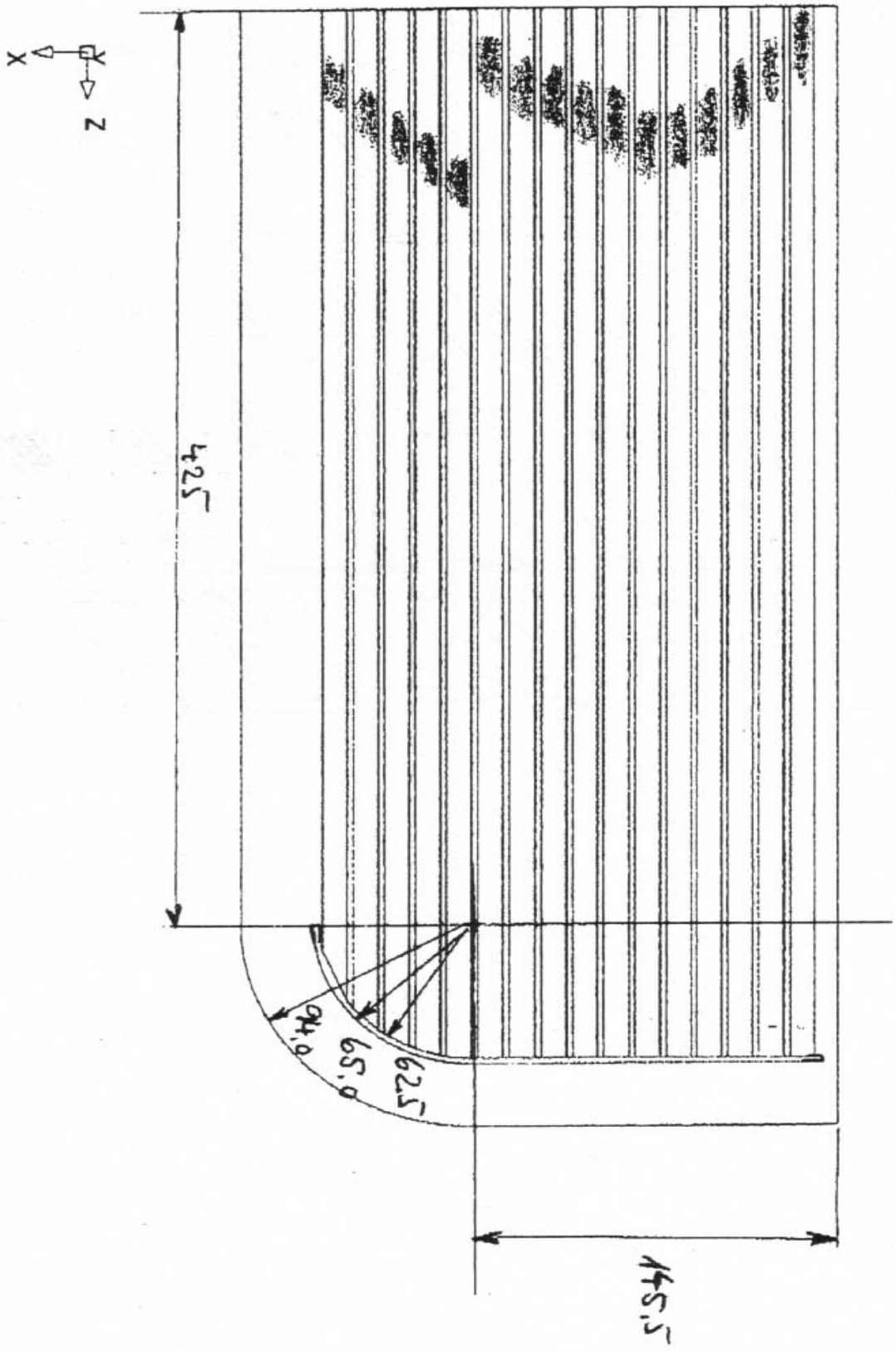
section 5.1.2) where stress concentrations are exaggerated in ANSYS, it is possible that the maximum stress results will reflect the instabilities and inaccuracies of the ANSYS program at such sharp corners, particularly in the plastic regime. This translates to an error factor in ANSYS that may need to be considered in evaluating the results in figure 5.4.3.

9. Including fillets at locations of stress intensity—such as in corners between surfaces—may mitigate the problem of exaggerated stress concentrations in ANSYS, giving more realistic results, improving the quality of the analysis, as well as lending greater validity to the solutions. This, however, would have the effect of significantly adding to the number of elements, thus hampering the computational efficiency of the solution.

**Appendix 1: engineering drawings of model (in mm)**







## REFERENCES

- [1] NM Ghoniem, JR Matthews, RJ Amadeo. "A Dislocation Model for Creep in Engineering Materials." *Res Mechanica* 29 (1990) 197-219.
- [2] T Heider, K Schleisiek, G Reimann, C Dellis, E Rigal. "Development of Manufacturing Processes for the ITER Helium-cooled Pebble Bed Blanket Test Module." *Fusion Engineering and Design* 39-40 (1998) 819-824.
- [3] S Hermsmeyer, J Fiek, U Fischer, C Köhly, S Malang, J Rey, Z Xu. "Revision of the EU Helium-cooled Pebble Bed Blanket for DEMO." To be published at the 16<sup>th</sup> ANS Topical Meeting on the Technology of Fusion Energy, 14-16 September 2004.
- [4] LV Boccaccini, S Hermsmeyer, J Reimann, U Fischer, Z Xu, C Köhly, J Rey. "Design of the Breeder Units in the New HCPB Modular Blanket Concept and Material Requirements." CBBI-11 Presentation, Tokyo, 15-17 December 2003.
- [5] MA Abdou. "Radiation Considerations for Superconducting Fusion Magnets." *J Nuclear Materials* 72 (1978) 147-167.
- [6] J Chiu. "Dislocation-based Finite Element Modeling of Elasto-plastic Material Deformation." Master of Science Thesis, University of California, Los Angeles. 2004.